CO_2 SELECTIVE CERAMIC MEMBRANE FOR WATER-GAS-SHIFT REACTION WITH CONCOMITANT RECOVERY OF CO_2

Final Report
For the period September 1, 2000 to March 31, 2005

Paul K. T. Liu
Project Director

July 15, 2005

PREPARED FOR THE UNITED STATES
DEPARTMENT OF ENERGY
Under Cooperative Agreement
No. DE-FC26-00NT40922

By
MEDIA AND PROCESS TECHNOLOGY, INC.
1155 William Pitt Way
Pittsburgh, PA 15238
and
UNIVERSITY OF SOUTHERN CALIFORNIA
Department of Chemical Engineering
Los Angeles, CA 90089-1211

Abstract

A high temperature membrane reactor (MR) has been developed to enhance the water-gas-shift (WGS) reaction efficiency with concomitant CO_2 removal for sequestration. This improved WGS-MR with CO_2 recovery capability is ideally suitable for integration into the Integrated Gasification Combined-Cycle (IGCC) power generation system. Two different CO_2-affinity materials were selected in this study. The Mg-Al-CO_3-layered double hydroxide (LDH) was investigated as an adsorbent or a membrane for CO_2 separation. The adsorption isotherm and intraparticle diffusivity for the LDH-based adsorbent were experimentally determined, and suitable for low temperature shift (LTS) of WGS. The LDH-based membranes were synthesized using our commercial ceramic membranes as substrate. These experimental membranes were characterized comprehensively in terms of their morphology, and CO_2 permeance and selectivity to demonstrate the technical feasibility. In parallel, an alternative material-base membrane, carbonaceous membrane developed by us, was characterized, which also demonstrated enhanced CO_2 selectivity at the LTS-WGS condition. With optimization on membrane defect reduction, these two types of membrane could be used commercially as CO_2-affinity membranes for the proposed application. Based upon the unique CO_2 affinity of the LDHs at the LTS/WGS environment, we developed an innovative membrane reactor, Hybrid Adsorption and Membrane Reactor (HAMR), to achieve ~100% CO conversion, produce a high purity hydrogen product and deliver a concentrated CO_2 stream for disposal. A mathematical model was developed to simulate this unique one-step process. Finally a bench-top reactor was employed to generate experimental data, which were consistent with the prediction from the HAMR mathematical model. In summary, the project objective, enhancing WGS efficiency for hydrogen production with concomitant CO_2 removal for sequestration, has been theoretically and experimentally demonstrated via the developed one-step reactor, HAMR. Future development on reactor scale up and field testing is recommended.

Executive Summary

A hybrid adsorption-membrane reactor (HAMR) process has been developed to enhance the water-gas-shift (WGS) reaction efficiency with concomitant CO_2 removal for sequestration. This improved WGS with CO_2 recovery capability is ideally suitable for integration into the Integrated Gasification Combined-Cycle (IGCC) power generation system. One adsorbent and two membranes were investigated in this project for their use for the proposed process. A bench-scale HAMR process was performed to demonstrate the process feasibility. Further, its performance was consistent with the prediction from the mathematical model developed in this project. In summary, the project objective, enhancing WGS efficiency for hydrogen production with concomitant CO_2 removal for sequestration, has been theoretically and experimentally demonstrated via the developed one-step reactor, HAMR. Future development on reactor scale-up and field-testing is recommended.

Two different CO_2-affinity inorganic materials were selected in this study. One of them, the Mg-Al-CO_3-layered double hydroxide (LDH), was investigated as an adsorbent or a membrane for CO_2 separation. Several *in-situ* techniques were applied in this study to investigate the thermal evolution behavior of the Mg-Al-CO_3 LDH material as a function of temperature and atmosphere. In the temperature range of 180 to 280°C, significant water and some CO_2 released while the layer structure of LDH remained. In the temperature range of 280 - 405°C, degradation of the LDH structure began. Further, in a cyclic experimental study simulating the LTS condition, about 1.3wt% CO_2 released in the 1st cycle. After 9th cycle, the reversible CO_2 affinity reached a steady state. About 1/3 of the original capacity was determined to be reversible. In summary, the CO_2 release at >190°C was experimentally verified to be reversible, an essential feature for preparing a commercially viable adsorbent or membrane.

The LDH adsorbent developed in this study demonstrated a sufficient adsorption capacity and intraparticle diffusivity at 180 to 250°C, suitable for low temperature shift (LTS) of WGS. Diffusivity constants and adsorption isotherms for carbon dioxide in Mg-Al-CO_3 LDH at 200 - 250°C were determined by the gravimetric method. Diffusivity constants determined by experiments and those obtained by molecular dynamic simulations are in good qualitative agreement. The experimental adsorption isotherms for CO_2 in LDH were studied with the Langmuir isotherm equation as well as various empirical adsorption isotherm equations. It was observed that the heterogeneity of the material and the interaction between CO_2 and LDH increased with temperature. Also it was found that the experimental data were nonlinearly fitted best with the Toth equation based on χ^2 values. Further, it was observed that the amount of CO_2 uptake and the (BET) surface area increased as the particle size decreased. When the uptake amount was normalized with the BET surface area, the uptake amount was fairly constant for all the range of particle sizes. The adsorption isotherm data with different particle sizes of LDH were studied with Langmuir isotherm and Langmuir-Freundlich equation. It was observed that the values of b_{CO_2} and n (constants used in the isotherms) were relatively constant for the whole range of particle sizes. The uptake and isotherm parameters and their best-fitted equation were used for simulating the CO_2 removal via LDH adsorbents in the HAMR reactor.

The technical feasibility of forming a CO_2-affintiy membrane with the LDH material has been demonstrated successfully. The two synthesis techniques and one post-treatment technique

were investigated in this project. Combining the observations from permeance, pore size distribution, EDAX and SEM, we concluded that the LDH crystals were deposited within the pore size of the starting membranes with the pore sizes of 40Å, 500 Å, and 0.2µm. This LDH-based membrane via in-situ crystallization was then post-treated by the CVD/I technique to minimize defects. The CO_2 permeance enhancement was exhibited in the membrane thus formed. For instance, the CO_2 permeance of 0.26 $m^3/m^2/hr/bar$ at 300°C was observed for one of the membranes after the post treatment by chemical vapor deposition/infiltration (CVD/I) technique. Further, our analysis indicated that >50% of the CO_2 permeance was likely attributed to the enhancement by the LDH materials. The balance was contributed by defects remaining in the membrane. The ideal selectivity for CO_2/N_2 ~1.6 at 100 to 300°C was obtained for the LDH membrane prepared via in-situ crystallization and the CVD/I post treatment. In comparison with the ideal selectivity through Knudsen diffusion of 0.8, the selectivity obtained here was about double of what delivered by the Knudsen diffusion. Evidently, the enhanced selectivity was not sufficient to be commercially viable. Optimization study was necessary to reduce the defect to a minimum via the membrane synthesis; thus, minimal post treatment is required to achieve the CO_2 enhancement without sacrificing permeance significantly. The other membrane synthesis technique, the slip casting technology developed here successfully developed a hydrotalcite membrane with the residual pore size of <40Å while maintaining most original permeance, i.e., 30 to 40 $m^3/m^2/hr/bar$, which could be an ideal starting material for the post treatment with CVD/I. No post treatment study was performed for this type of the LDH membrane due to the time constraint. Additional work with the focus on minimization of defects is recommended to upgrade the CO_2 selectivity and permeance for future commercial use.

In parallel, an alternative membrane, carbonaceous membrane developed by us, was characterized, which also demonstrated enhanced CO_2 selectivity at the LTS-WGS condition. This CO_2 affinity membranes demonstrated a higher selectivity for CO_2/N_2, i.e., 4 to 10, up to 220°C, which was much beyond the Knudsen selectivity. Surface affinity of the membrane toward the CO_2 was identified as the dominating mechanism at this operating temperature range. Selectivity at this level is comparable or higher than the selectivity of CO_2/N_2 reported in the literature at the proposed reaction temperature. Additional study including characterization of this type of membrane in a mixture environment is recommended for future development.

Based upon the unique CO_2 affinity of these materials at the LTS/WGS environment, we investigated a novel reactor system, termed the HAMR, for hydrogen production through water gas shift reaction with concomitant CO_2 removal for sequestration. The HAMR combined the reaction and membrane separation steps with adsorption on the membrane feed or permeate side. A mathematical model was developed to simulate this unique one-step process. The reactor characteristics were investigated for a range of temperature, pressure, and other experimental conditions relevant to the aforementioned applications and compared with the behavior of the traditional packed-bed reactor, the conventional membrane reactor (MR) and an adsorptive reactor (AR). The HAMR outperformed all of the other more conventional reactor systems. It exhibited enhanced CO conversion, hydrogen yield, and product purity. The disadvantage of the HAMR system was, similar to that for the ARs, in that they required regeneration of the spent adsorbent, for continuous operation. The HAMR might require a

dual reactor system, where one of the reactors is in operation while the other reactor is being regenerated. Our preliminary experimental results were consistent with the prediction with the mathematical model prediction. HAMR, offers potential to achieve ~100% CO conversion, produces a high purity hydrogen product and delivers a concentrated CO_2 stream for disposal. According to our preliminary economic analysis, about 10% reduction in hydrogen production cost could be achieved under the selected operating condition. More importantly, significant capital cost reduction potential can be realized as a result o the process intensification by the proposed HAMR system. In summary, the project objective, enhancing WGS efficiency for hydrogen production with concomitant CO_2 removal for sequestration, has been theoretically and experimentally demonstrated via the developed one-step reactor, HAMR. Future development on reactor scale-up and field-testing is recommended.

Table of Contents

Chapter **Page**

List of Figures

Figure **Page**

List of Figures (continued)

List of Figures (continued)

List of Figures (continued)

List of Tables

List of Tables (continued)

Chapter 1

Hydrogen Production with Concomitant CO_2 Removal for Sequestration - Introductory Remarks

Since substantial (1/4-1/3) anthropogenic emissions of carbon to the atmosphere result from power generation [1,4], control of CO_2 emission from this particular source is considered one of the most efficient strategies to achieve the national goal of greenhouse gas management. This centralized, instead of dispersed, CO_2 source will provide an attractive opportunity to implement a cost-effective treatment solution. However, the conventional end-of-the-pipe treatment approach, i.e., capture of CO_2 after combustion with air, is not considered economical because the gas volume increases tremendously (~ 3 times) after combustion. According to the literature, this approach costs ~$40/ton of carbon (for a 500 MW fossil fuel-fired power plant, [1]), not including the additional cost for transportation and disposal of CO_2. To develop a cost acceptable solution for CO_2 sequestration, a new direction has been suggested [1] which requires a combination of the following:

- increased base power plant efficiencies,
- reduced capture process energy needs, and
- integration of the capture process with the power plant.

Under this direction we proposed the development of a high temperature CO_2-selective membrane as a reactor (MR), which can enhance the water-gas-shift (WGS) reaction efficiency while recovering CO_2 simultaneously for disposal.

The MR can offer significant advantages to the WGS reaction, mainly (i) reduced capital cost because the high conversion can be achieved in a single stage, (ii) reduced operating cost because steam usage can be reduced, and (iii) reduced CO_2 sequestration cost because CO_2 can be separated from the MR simultaneously. A comprehensive analysis performed by the European Consortium [3] estimated that the net efficiency of the IGCC process with integrated WGS-MR is 42.8% (based upon lower heating value, LHV) with CO_2 recovery (80% based on coal input). This figure is compared with 40.5% (LHV) for an IGCC with conventional CO_2 removal. Therefore, CO_2 separation with significant improvement in power generation efficiency can potentially be delivered by the implementation of the WGS-MR.

The specific affinity to CO_2 of our proposed MR is accommodated by the two unique membrane materials selected in this study. More importantly, they present several unique advantages in membrane synthesis over other existing or emerging materials. This improved WGS-MR w/ CO_2 recovery capability is ideally suitable for integration into the Integrated Gasification Combined-Cycle (IGCC) power generation system. Thus, the high purity hydrogen (high pressure and CO_2 -free) produced from the IGCC can be used either as a product for power generation via a turbine or a fuel cell, or as a reactant for fuel and chemical production.

To achieve this project objective, we proposed the development of MR process to enhance the WGS conversion with concomitant separation of CO_2. Two synthesis concepts on the CO_2-selective ceramic membrane have been pursued under this project: (i) imbedding the Al-Mg-CO_3 layered double hydroxides (LDH) material with CO_2 transport channels, and (ii) depositing carbonaceous material with surface affinity to CO_2 membrane, into the porous structure of the Al_2O_3 ceramic membrane available from us. In this project, we performed synthesis and characterization of these base materials and further evaluated their technical feasibility for the formation of CO_2 affinity membranes. Then, an innovative hybrid reactor process concept was developed and evaluated for its hydrogen production with the concomitant CO_2 removal. Finally a bench-scale WGS reactor study was conducted to experimentally demonstrate the proposed MR concept and its benefit to CO_2 recovery. This project report summarizes rationals, experimental approach, results and discussion, and conclusions for each individual technology element involved in this unique process.

Literature Cited

1. Herzog, H., E. Drake, E. Adams, CO2 Capture, Reuse, and Storage Technologies for Mitigating Global Climate Change, Final Report, DOE Order No. DE-AF22-96PC01257 January 1997.
2. US DOE, Program Solicitation No. DE-PS26-99FT40613, Sep. 8, 1999.
3 Bracht, M., Alderliesten, PT., Kloster, R., Pruschker, R., Haupt, G., Xue, E., Ross, JR., Koukou, M.K., Papayannakos, N., Energy Conservation and Management, 38, 8159 (1997).
4. US DOE, Working Paper on Carbon Sequestration Science and Technology, February 1999

Chapter 2

Thermal Evaluation Study of Mg-Al-CO_3 Layered Double Hydroxides

2.1 Introduction

To develop an CO_2-affinity adsorbent or membrane for our proposed water gas shift reaction at ~200 to 400°C, knowledge on the thermal evolution behavior of this material and its corresponding surface and structure change are essential. In this chapter, the thermal evolution behavior of one of the two selected materials, the Mg-Al-CO_3 LDH is presented using various *in-situ* techniques, including DRIFTS, TG/DTA, TG/MB-MS, and HTXRD. DRIFTS is a sensitive and powerful technique that was utilized in this study to monitor *in-situ* the changes of functional groups of the Mg-Al-CO_3 LDH as a function of temperature and other experimental conditions. *In-situ* TG/DTA techniques were used to monitor the weight and energetic changes of the Mg-Al-CO_3 LDH as a function of temperature. Combining DRIFTS with TG/TDA provides quantitative insight into functional group changes at various temperatures. In addition *in-situ* TG/MB-MS techniques were used to monitor gaseous products generated during their thermal evolution as a function of temperature and other conditions. Combining DRIFTS with TG/MB-MS provides additional quantitative insight into functional group changes at various conditions. Finally, *in-situ* HTXRD was employed to detect the structural changes of Mg-Al-CO_3 LDH as a function of temperature. The results obtained from these *in-situ* techniques allow us to comprehensively characterize the surface and structure change as a function of temperature and eventually develop a model for the thermal evolution behavior of the Mg-Al-CO_3 LDH material, which is essential to design intelligently a CO_2-affinity membrane.

2.2 Experimental

The LDH sample was provided by the Media and Process Technology, Inc., of Pittsburgh, PA. Its composition is $Mg_{0.71}Al_{0.29}(OH)_2(CO_3)_{0.15}{\cdot}0.46(H_2O)$ (hereinafter referred to as LDH1), as determined by ICP and TGA. Experimental methods performed in this chapter are briefly described below:

- DRIFTS spectra were recorded *in-situ* using a Genesis II (Mattson, FT-IR) instrument equipped with a DRIFTS COLLECTOR™ II chamber (SpectraTech, Inc.) capable of operating under high temperatures (up to 900 ^oC) and pressures (up to 1500 psi). The chamber windows are made of ZnSe to withstand these conditions, and to allow for better infrared transmission. A controller is used to control the chamber temperature utilizing a ceramic heater and a thermocouple in intimate contact with the sample. With this chamber, the temperature and the sample environment can be easily controlled. The experimental operating conditions were a DRIFTS scan-range from 4000 cm^{-1} to 500 cm^{-1}, scan numbers 16, and a scan resolution of 2 cm^{-1}. The spectra were calibrated for background with KBr. To obtain a strong signal intensity and better resolution for quantitative measurements, the sample was first ground to 2-10 μm, diluted with KBr to

5~10% wt., placed in the sample cup and leveled with a spatula. Experiments were carried out in an inert gas atmosphere. The temperature was raised at a rate of 0.5 ^{o}C/s, and spectra were recorded at different temperatures about 20 ^{o}C apart.

- For the thermal evolution of LDH's study, the thermogravimetric (TG) curve was recorded on a Pyris 1 TGA HT instrument (PE Company) by heating the sample from 50 to 600 ^{o}C in an Ar atmosphere, at a rate of 5 ^{o}C/min, and an Ar flow rate of 20 ml/min. Differential thermal analysis (DTA) was performed with a DTA 7 instrument (PE Company) at the same conditions as TG. For *in-situ* TG/MB-MS techniques, the thermogravimetric (TG) curve was recorded on a Cahn TGA 121 instrument, and TG/MB-MS instrument that is custom-made, using a MKS UTI 100C Precision Gas Analyzer.

- HTXRD experiments were carried out in the temperature range 30 - 650^{o}C under vacuum (10^{-2} Torr) using a Siemens D-5000 X-ray diffractometer equipped with a Buhler high-temperature chamber HDK 1.4. The chamber is made of stainless steel with Be-windows for X-ray transmission and Ta thermal shields acting as the isothermal block. The sample and its surroundings were heated by Pd heaters at a rate of 0.5 ^{o}C/s; the spectra were recorded at different temperatures, typically 20 ^{o}C apart. The sample was equilibrated at any given temperature for 30 min. The Cu K_α line was used for the X-ray source with a monochromator positioned in front of the detector. Scans were performed over a 2θ range from 5^{o} to 75^{o}.

2.3 Results and Discussion

The thermal evolution pattern obtained with the use of the above instrumentations is discussed below:

Spectra Assignment…Figure 2.1 compares the DRIFTS and FT-IR spectra of the LDH1 at room temperature in Ar. It shows that all key bands in the DRIFTS spectra for the LDH1 are in the same position as those in the FT-IR spectra. The intensities of the DRIFTS signals are sufficiently strong to clearly identify all the important functional groups. In accordance with prior FT-IR studies[1,2], the DRIFTS bands were assigned to the following groups:

(1) The DRIFTS signal at ~3470 cm^{-1} is due to the OH^- group vibration in the Mg-Al-CO_3 LDH sample;
(2) the DRIFTS signal at ~3070 cm^{-1} is due to hydrogen bonding between water and the carbonate species in the interlayer space of the Mg-Al-CO_3 LDH sample;
(3) the DRIFTS signal at ~1620 cm^{-1} is due to the H_2O bending vibration of interlayer water in the Mg-Al-CO_3 LDH sample and;
(4) The DRIFTS signals at ν_3=1370cm^{-1}, ν_2=940cm^{-1}, and ν_4=680cm^{-1} at room temperature are due to the CO_3^{2-} group vibration bands in the Mg-Al-CO_3 LDH sample; the CO_3^{2-} group in the hydrotalcite behaves more like it would in a water solution, in which the vibration bands of CO_3^{2-} are observed at ν_3=1415cm^{-1}, ν_2=880cm^{-1}, and ν_4=680cm^{-1}. No ν_1 mode vibration at ~1080cm^{-1}, and no

splitting of the ν_3 band are observed. The splitting of the ν_3 band and the ν_1 mode vibration band are usually generated from the symmetry degradation, which results from the interaction between CO_3^{2-} and Mg^{2+}. This means that CO_3^{2-} in the Mg-Al-CO_3 LDH sample at room temperature has a very weak, if any, direct interaction with positive ions, such as Mg^{2+} and Al^{3+}.

Thermal Evolution based upon DRIFTS…Based on the above band assignments, one can use the *in-situ* DRIFTS technique to characterize the LDH structural evolution process, especially the changes of the functional groups of the Mg-Al-CO_3 LDH sample as a function of temperature. The *in-situ* DRIFTS results are shown in Figure 2.2, for which the LDH1 was treated in Ar. In these experiments, starting from room temperature, the sample temperature was increased at a rate of 0.5 ^oC/s. Every 20 ^oC or so the temperature increase was on-hold, and the DRIFTS spectra would be recorded after keeping the sample isothermal for a period of ~2 min. The testing was continued until the temperature of the sample had reached 580 ^oC. From Figure 2.2 one can draw the following conclusions:

(1) The intensities of the interlayer water bands at 3070 cm^{-1} and 1620 cm^{-1} gradually decrease with increasing temperature, and disappear around 190^oC. This means that increasing amounts of interlayer water in the LDH1 are removed with increasing temperature. In the presence of Ar beyond 190 ^oC the water that remains in the sample is below the detection limit of the DRIFTS instrument.
(2) The intensity of the OH^- vibration band at 3470cm^{-1} begins to decrease at 190 ^oC, and completely disappears at 440 ^oC. This suggests that in the presence of Ar dehydroxylation of LDH1 begins at 190 ^oC; by the time the temperature reaches 440 ^oC the concentration of the remaining OH^- groups is below the detection limit of the DRIFTS instrument.
(3) The band at 1370 cm^{-1} for the CO_3^{2-} ν_3 vibration begins to decrease in size as the temperature increases, and also shifts to ~ 1350 cm^{-1}. Gradually a band at 1530 cm^{-1} begins to form at temperatures higher than 170 ^oC. The band size at the lower wave number (~1350 cm^{-1}) decreases as the temperature increases (and so are the peaks at 940 and 680 cm^{-1}). This is to be expected as the amount of interlayer water decreases and, as a result, the CO_3^{2-} group begins to interact more strongly with the backbone of the hydrotalcite itself. For comparison purposes, Figure 2.3 shows the DRIFTS spectrum of $MgCO_3$. The behavior of the two bands at 1499 and 1425 cm^{-1} qualitatively mirrors that of the bands at 1530 and 1350 cm^{-1}. On the other hand, the state of CO_3^{2-} in the hydrotalcite is distinctly different from that in $MgCO_3$. Note that bands corresponding to the ν_3 vibration of CO_3^{2-} in $MgCO_3$ are at different positions, namely 1499cm^{-1} and 1425cm^{-1}. In Figure 2.3, one observes the ν_1 vibration band of CO_3^{2-} in $MgCO_3$. This band is not present in Figure 2.2. At higher temperatures all peaks corresponding to CO_3^{2-} species in Mg-Al-CO_3 LDH disappear. This is consistent with the MS data (see the discussion below), which show that by that temperature all CO_3^{2-} has left the hydrotalcite structure as CO_2.

Figure 2.4 summarizes the *in-situ* DRIFTS results of Figure 2.2, indicating the fraction of each particular species that was removed at a given temperature. The calculations based on the peak area of the corresponding species recorded at different temperatures. The 3470 cm^{-1} band represents the OH^- group, and the 3070 cm^{-1} and 1620 cm^{-1} bands represent the interlayer water. For CO_3^{2-}, since the DRIFTS band at 1370cm^{-1} at lower temperatures was split into two DRIFTS bands, i.e., 1530cm^{-1} and 1350cm^{-1}, in the quantitative analysis, the fraction removed was calculated only at temperatures higher than 180 °C using the 1530cm^{-1} and 1350cm^{-1} band to represent CO_3^{2-}. 100% removal in Figure 2.4 corresponds to the point when the particular band is no longer detectable by DRIFTS. It can be seen in Figure 2.4 that the interlayer water starts to disappear at 70 °C, with the band no longer detectable at 190 °C. For the OH^- groups, there is a noticeable difference in the slope of the removal rate between the temperature ranges 190 - 250°C and 250 – 440 °C, suggesting, perhaps, that in these two temperature ranges the OH^- group finds itself in two different environments in the Mg-Al-CO_3 LDH sample. Figure 2.4 also indicates that most of the CO_3^{2-} was removed in the temperature range 390 - 580°C. These results were also confirmed by *in-situ* MS and TG/MS experiments. Figure 2.5, for example, shows the results of *in-situ* MS analysis. It indicates that H_2O is continuously removed from the Mg-Al-CO_3 LDH1 sample until 420 °C, which is consistent with the results of DRIFTS, shown in Figure 2.4. *In-situ* DRIFTS is a powerful technique to monitor the changes of the functional groups in Mg-Al-CO_3 LDH sample as the temperature changes.

Thermal Evolution based upon TG/DTA/MS…*In-situ* TG/MS and TG/DTA, as previously noted, provide complimentary technical information. Figure 2.6 shows, for example, the results of *in-situ* TG/MS analysis. It indicates that a relatively small amount of CO_2 (~11.5%) from the LDH1 was detected in the temperature range of 190 – 390 °C, and most of the CO_2 (~88.5%) from the Mg-Al-CO_3 LDH was detected in the temperature range of 390 – 580 °C. These results are consistent with the results of DRIFTS, shown in Figure 2.4. Figure 2.7 shows the corresponding results of the TG/DTA analysis of the Mg-Al-CO_3 LDH1 sample as a function of temperatures in an inert gas atmosphere.

In-situ DRIFTS with TG/MS for 70 – 190°C…Combining the *in-situ* DRIFTS results with the TG/MS observations, one can draw quantitative conclusions concerning the behavior of the various functional groups. One can conclude, for example, that in Figure 2.6 the first weight loss, ~13.5% by weight, in the temperature range of 70 - 190 °C should be mostly due to the interlayer water in the Mg-Al-CO_3 LDH, together with relatively smaller amounts of CO_2 and H_2O resulting from the desorption of the OH^- group. The theoretical weight fraction of the interlayer water in Mg-Al-CO_3 LDH1 with the reported composition of $Mg_{0.71}Al_{0.29}(OH)_2(CO_3)_{0.15}.0.46H_2O$ is calculated to be 10.84 % by weight. The difference (2.66 % by weight) between the experimental value (13.5 % by weight) and the theoretical value (10.84 % by weight) should be attributed to the contribution of CO_2 and H_2O from the OH^- group, because there are, indeed, small amounts of CO_2 and H_2O from the OH^- group that were removed in the temperature range of 70°C to 190°C, as shown in Figures 2.4 and 2.6. The DTA results (Figure 2.7) show no distinct peaks in the temperature range of 70 - 190°C, which is consistent with

the conclusion that the removal of interlayer water, which is physically adsorbed in the nano-slits between the layers of Mg-Al-CO_3 LDH, is predominantly responsible for the sample weight loss in this region.

In-situ DRIFTS with TG/MS for 190-400°C…The second distinct weight loss region of 22.17 wt.% (Figure 2.7) is in the temperature range ~190 - ~400 ^oC. It is accompanied by the evolution of H_2O and CO_2 species (see Figures 2.4 and 2.6), and various heat flows (Figure 2.7). The first small heat flow shoulder peak (endothermic) is centered at ~205^oC, and seems to be coincident with the change of the 1370 cm^{-1} peak in Figure 2.2. The mass spectrometric data indicate the evolution of CO_2 and some H_2O in this region. From ~190 to ~220 ^oC the weight change is ~ 0.2 %, of which 0.08 % corresponds to CO_2 and 0.12 % to H_2O. The small heat flows are indicative that the OH^- and CO_3^{2-} that are exchanged in this region may be physically bound in the LDH sample. Between ~220 and ~ 400 ^oC, there is a 21.97 % weight change; there are also two characteristic endothermic flows in this region, one centered at ~255 ^oC and the other at ~340 ^oC. The DTA data seem to be consistent with the DRIFTS data, which indicate potentially two types of OH^- groups that are removed in the same approximate region of temperatures. In order to clarify the properties of these two types of OH^- groups, TG/DTA experiments with pure $Al(OH)_3$ and pure $Mg(OH)_2$ samples were also performed; the results are shown in Figures 2.8 and 2.9. Figure 2.8 indicates that the OH^- group associated with Al^{3+} is lost in the temperature range ~190 - ~ 300 ^oC, and two heat flow peaks (endothermic) are observed in the same region. Figure 2.9 shows that the OH^- group associated with Mg^{2+} is removed in the temperature range 300 – 405 ^oC; only one heat flow peak (endothermic) is observed at this case. Comparing Figure 2.7 with Figures 2.8 and 2.9, one observes that the thermal behavior of Mg-Al-CO_3 LDH1 in Figure 2.7 is a composite of the thermal behavior of $Al(OH)_3$ and $Mg(OH)_2$. The weight loss in the temperature range 190 - 300 ^oC is ~8.93 %. Of this 0.19 % corresponds to CO_2 and 8.74 % to the removal of H_2O, which likely results from Al-(OH)-Mg OH^- groups. Between 300 ^oC and 405 ^oC the weight loss is ~13.24 %. Of this 0.72 % corresponds to CO_2 and 12.52 % to the removal of H_2O, which for this case, more likely, results from Mg-(OH)-Mg OH^- groups. Assuming that Al^{3+} associates only with OH^- groups, the total weight change one would expect due to the evolution of H_2O from OH^- is 10.37 %. This compares favorably with the 8.74 % change due to water measured in the region of 190 – 300 ^oC. The weight change one would expect due to the evolution of H_2O from the OH^- groups associated with Mg^{2+} is 13.20 %. The experimental value in the region 300 – 405 ^oC is 12.52 %, which compares favorably with the calculated value.

In-situ DRIFTS with TG/MS for 405 -580°C…The total weight loss from 405 to 580 ^oC is 7.33 %, which can be attributed to the removal CO_2 from CO_3^{2-} in the Mg-Al-CO_3 LDH, because almost no water was detected in this temperature range by *in-situ* MS. This brings the total weight loss due to CO_2 to 8.32 %, as compared with the calculated value of 7.15%.

Proposed Model for Structure Change…Based on the results of *in-situ* DRIFTS coupled with the *in-situ* TG/DTA and TG/MS studies, a model is proposed for the evolution of the structure of the Mg-Al-CO_3 LDH sample under an inert atmosphere (Figure 2.10). In

Figure 2.10 five distinct stages were identified during the thermal evolution of this particular Mg-Al-CO_3 LDH sample. The original Mg-Al-CO_3 LDH sample is referred to as Stage A; Stage B develops from Stage A by the removal of the loosely held interlayer water in the temperature range 70 - 190 ^oC; Stage C evolves from Stage B by the removal of OH^- groups, likely bonded in a bridge Al-(OH)-Mg configuration, in the temperature range 190 - 300 ^oC; Stage D was achieved from Stage C by the removal of OH^- groups, likely bonded mostly with Mg^{2+} (Mg-(OH)-Mg) in the temperature range 300 - 405 ^oC; Stage E is obtained by the decarbonation of Stage D in the temperature range 405 - 580 ^oC.

HTXRD…It is also interesting to investigate how the changes in the number and type of functional groups with temperature manifest themselves in changes in the crystal structure of the Mg-Al-CO_3 LDH1 sample. In order to study this, *in-situ* HTXRD has been utilized. Figure 2.11 shows the HTXRD patterns of the Mg-Al-CO_3 LDH treated at different temperatures. There are five temperature regions that can be identified based on the HTXRD patterns, i.e., (1) 30 ^oC = T = 140 ^oC, (2) 140 ^oC = T = 180 ^oC, (3) 180 ^oC = T = 280 ^oC, (4) 280 ^oC = T = 360 ^oC, and (5) 360 ^oC = T = 650 ^oC.

For the first temperature region 30 - 140 ^oC, all the HTXRD patterns are attributed to the hydrotalcite-like structure, as reported by Kanezaki[3]. The intensities of HTXRD lines are strong, and stay almost unchanged with increasing temperature, meaning that the LDH structure is well preserved in this temperature region. More detailed analysis of HTXRD data has shown that the basal spacing of

Table 2.1 The changes in the basal spacing of Mg-Al-CO_3 LDH with temperature calculated from the HTXRD patterns.

T,^oC	30	50	70	100	120	140		160		180	
2θ	11.60	11.60	11.60	11.69	11.69	11.79	13.4	12.06	13.4	12.06	13.4
d, Å	7.63	7.63	7.63	7.56	7.56	7.50	6.59	7.33	6.59	7.33	6.59

Table 2.2 The changes in the basal spacing of Mg-Al-CO_3 LDH with temperature calculated from the HTXRD patterns.

T, ^oC	200	220	240	260	280	300	320	340	360
2?	13.5	13.6	13.8	13.9	13.9	14.0	14.0	14.0	14.0
d, Å	6.54	6.50	6.40	6.36	6.36	6.31	6.31	6.31	6.31

LDH has decreased from 7.63 Å to 7.5 Å, as the temperature increased from 30 to 140 ^{o}C (Table 2.1).

In the second temperature region 140 – 180 ^{o}C, the strong X-ray diffraction line at 11.6 starts shifting towards ~12^{o}, and a new line appears around 13.4^{o}, which intensifies with increasing temperature. This X-ray diffraction line was indexed as 001 by Kanezaki[3]. Based on the X-ray diffraction spectrum one can identify two different co-existing crystal phases of Mg-Al-CO_3 LDH: Phase I with a basal spacing ranging from 7.5 Å to 7.3Å, and Phase II with basal spacing of ~ 6.6Å. The basal spacing of Phase I is approximately equal to the sum of the thickness of one layer of Mg-Al-CO_3 LDH (4.8 Å) and the interlayer distance of Mg-Al-CO_3 LDH (~3.0 Å), as reported, for example, by Cavini, Trifiro, & Vaccari[4]. By assuming the same thickness of one layer of Mg-Al-CO_3 LDH (4.8 Å) for both phases the interlayer distance of Phase II of Mg-Al-CO_3 LDH is calculated to be 1.79 Å, a decrease from the 2.83 Å interlayer distance of Phase I. The decrease of the interlayer distance can be attributed to the shrinkage of the layers of Mg-Al-CO_3 LDH due to the removal of interlayer H_2O, since only interlayer H_2O was removed (DRIFTS and TG/DTA results) in the temperature range 70 - 190^{o}C.

In the third temperature region 180 - 280^{o}C, the X-ray diffraction line at ~12^{o} gradually disappears, and the line at ~13.4^{o} becomes stronger and simultaneously shifts towards 13.9^{o}. This means that, in this region, Phase I transforms to Phase II. With increasing temperature, the basal spacing of Phase II decreases from 6.59 Å to 6.36 Å. Simultaneously, the other X-ray diffraction lines of hydrotalcite begin to weaken in this temperature region, but the hydrotalcite structure stays intact though the interlayer spacing has decreased. This is consistent with the DRIFTS and TG/TDA data, which indicate removal of Al-(OH)-Mg OH^- groups, while the OH^-/CO_3^{2-} groups likely bonded with Mg^{2+} still remain intact; the LDH, thus, retains the brucite-like structure, as shown in Figure 2.10 (Stage C). The decrease of the basal spacing is attributed to the decrease in the thickness of the Mg-Al-CO_3 LDH layer due to the removal of Al-(OH)-Mg OH^- groups.

In the fourth temperature region 280 - 360 ^{o}C, the intensity of the diffraction line at ~14^{o} decreases, the line disappearing when the temperature exceeds 360 ^{o}C. This means that the layered structure of Mg-Al-CO_3 LDH falls apart above 360 ^{o}C, consistent with the observation that the OH^-/CO_3^{2-} groups (likely bonded with Mg^{2+}) begin to leave at 280 ^{o}C and are completely removed at 405 ^{o}C (Stage D), as shown in Figure 2.10. Removing these groups results in a collapse of the brucite-like layers and the Mg-Al-CO_3 LDH layered structure.

For the fifth temperature region 360 - 650^{o}C, the HTXRD results for temperatures higher than 360 ^{o}C are not shown in Figure 2.11, because all these patterns are similar to those shown for 360 ^{o}C. No HTXRD peaks are observed in this temperature region. At this stage (Figure 2.10) a solid solution of MgO and Al_2O_3 is obtained by decarbonation of the Stage D compound in the temperature range 410 - 580^{o}C.

2.4 Conclusions

In-situ DRIFTS, DTA, TG/MS and HTXRD techniques were applied in this study to investigate the thermal evolution behavior of the Mg-Al-CO_3 LDH as a function of temperature and atmosphere. Based on the results obtained from the individual and combined techniques, key conclusions may be drawn as follows:

(1) In the temperature range of 70 - 190^{o}C, loosely held interlayer water is lost, and there are two different co-existing crystal phases of Mg-Al-CO_3 LDH present, i.e., Phase I with a basal spacing ranging from 7.5 Å to 7.3Å, and Phase II with basal spacing of ~ 6.6Å. The LDH structure remains intact.

(2) In the temperature range of 190 - 280^{o}C, the OH^- group bonded with Al^{3+} begins to disappear at 190 ^{o}C, and is completely lost at 280^{o}C. In this temperature region, Phase I is transformed into Phase II. In addition a small amount of CO_2 releases.

(3) In the temperature range 280 - 405^{o}C, the OH^- group bonded with Mg^{2+} begins to disappear at 280^{o}C and is completely lost at 405^{o}C. Degradation of the LDH structure is observed in this region. Again a small amount of CO_2 releases.

(4) Finally, in the temperature range 405 - 580^{o}C, CO_3^{2-} loss begins and is completed at 580^{o}C. In this temperature range the material becomes a metastable mixed solid oxide solution.

Based upon the CO_2 loss vs temperature profile, a real opportunity exists in utilizing the LDH materials as a CO_2 affinity material at temperature >190°C. The LDH maintains its double layer structure up to 280°C. Beyond this temperature, the degradation of the LDH structure was observed under the inert atmosphere studied here. However, the LDH structure can be restored when the exposed atmosphere is appropriate. The CO_2 release at >190°C will be further verified with regard to its reversibility in Chapter 3, an essential feature for being used as a commercially viable adsorbent or membrane.

Literature Cited

1. Hibino, T.; Yamashita, Y.; Kosuge, K.; Tsunashima, A. Decarbonation behavior of Mg-Al-CO_3 hydrotalcite-like compounds during heat treatment. *Clays and Clay Min.*, **1995**, *43(4)*, 427.
2. Perez-Ramirez, J.; Mul, G.; Kapteijn, F.; Moulijn, J. A. (2000). Comments on "Infrared emission spectroscopic study of the thermal transformation of Mg-, Ni-, and Co-hydrotalcite catalysts" [*Appl. Catal A:General*, **1999,** *18*, 61]. *Appl. Catal, A: General*, **2000**, *204*, 256.
3. Kanezaki, E. Thermal behavior of the hydrotalcite-like layered structure of Mg and Al-layered double hydroxides with interlayer carbonate by means of *in-situ* powder HTXRD and DTA/TG. *Sol. State Ion.*, **1998**, *106(3-4)*, 279.
4. Cavini, F.; Trifiro, E.; Vaccari, A. Hydrotalcite-type anionic clays – preparation, properties and applications. *Cat. Today*, **1991**, *11*, 173.

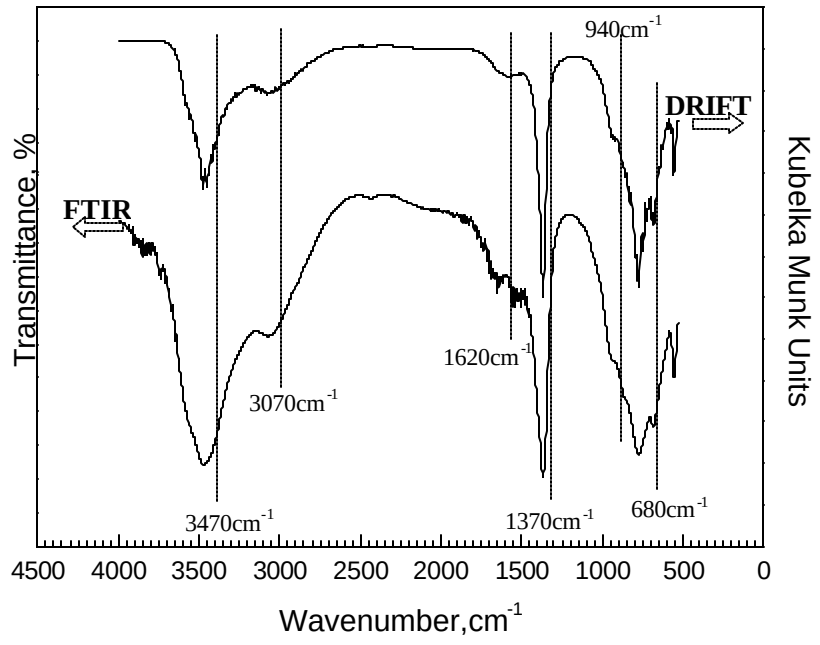

Figure 2.1 Comparison between the DRIFTS and FTIR results of Mg-Al-CO_3 LDH.

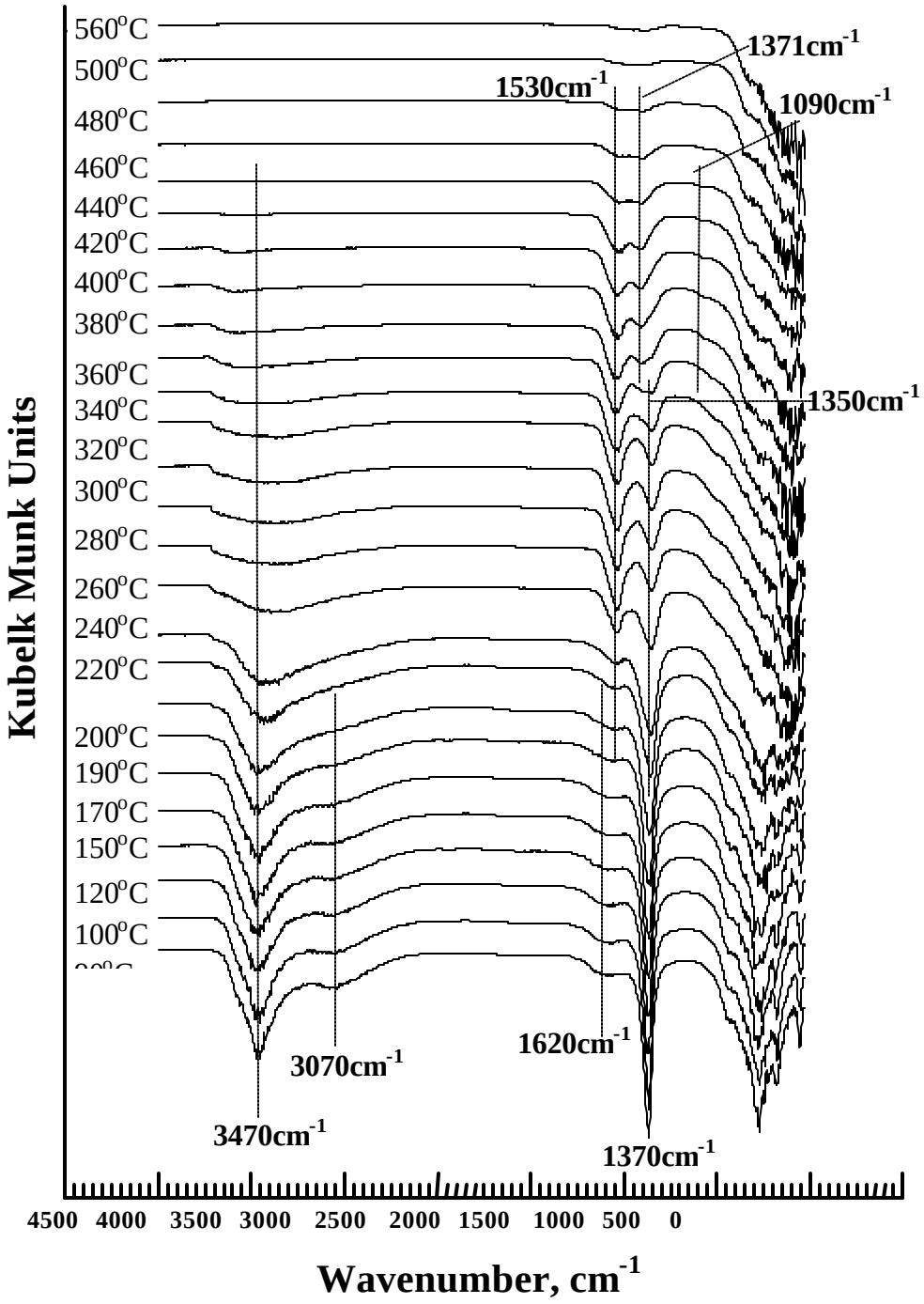

Figure 2.2 *In-situ* DRIFTS of Mg-Al-CO_3 LDH as a function of temperature.

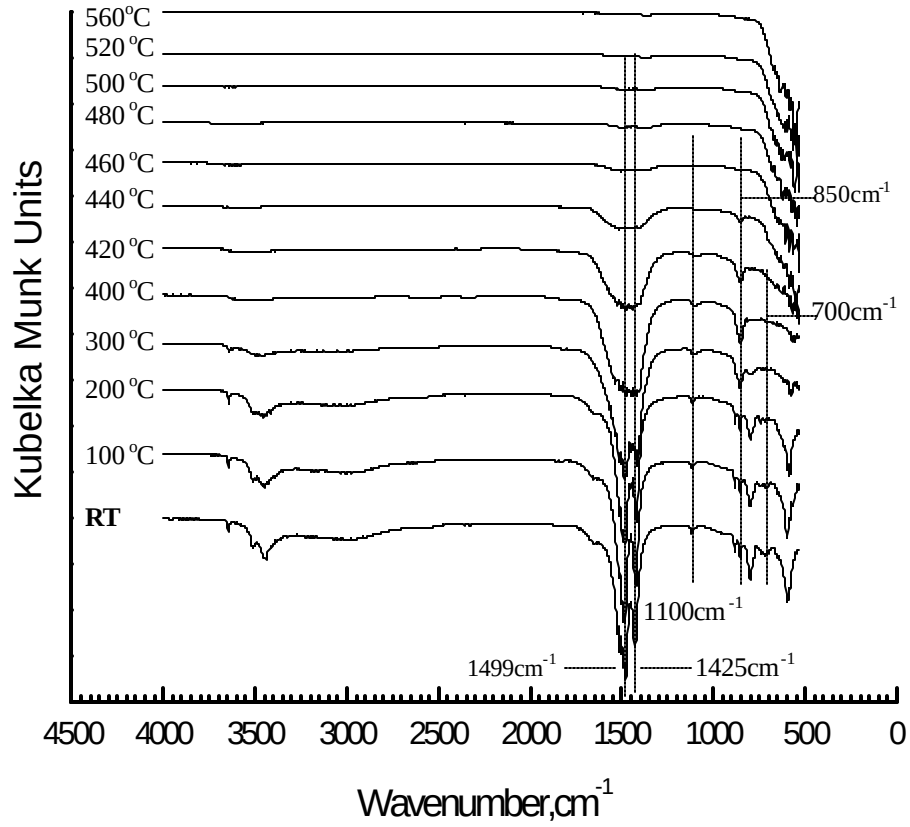

Figure 2.3 *In-situ* DRIFTS of $MgCO_3$ as a function of temperature.

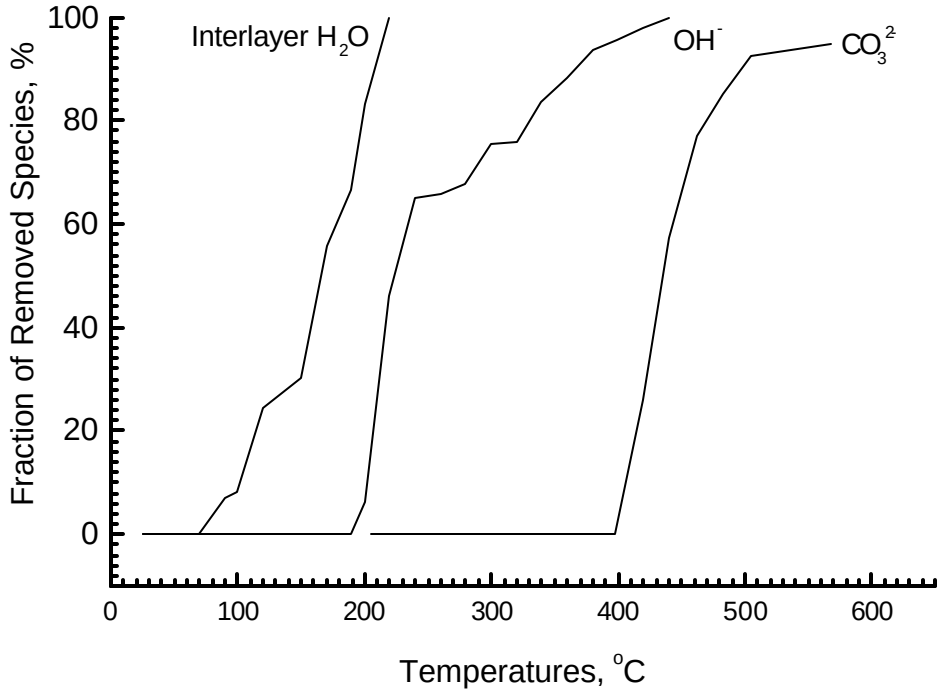

Figure 2.4 Fraction of species removed from Mg-Al-CO_3 LDH as a function of temperature.

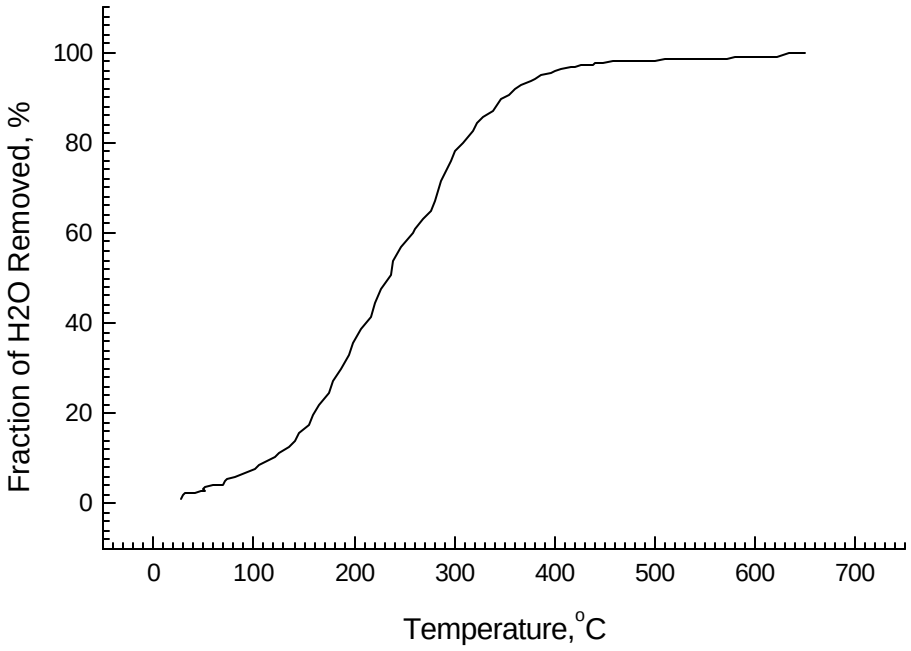

Figure 2.5 *In-situ* MS of Mg-Al-CO_3 LDH as a function of temperature.

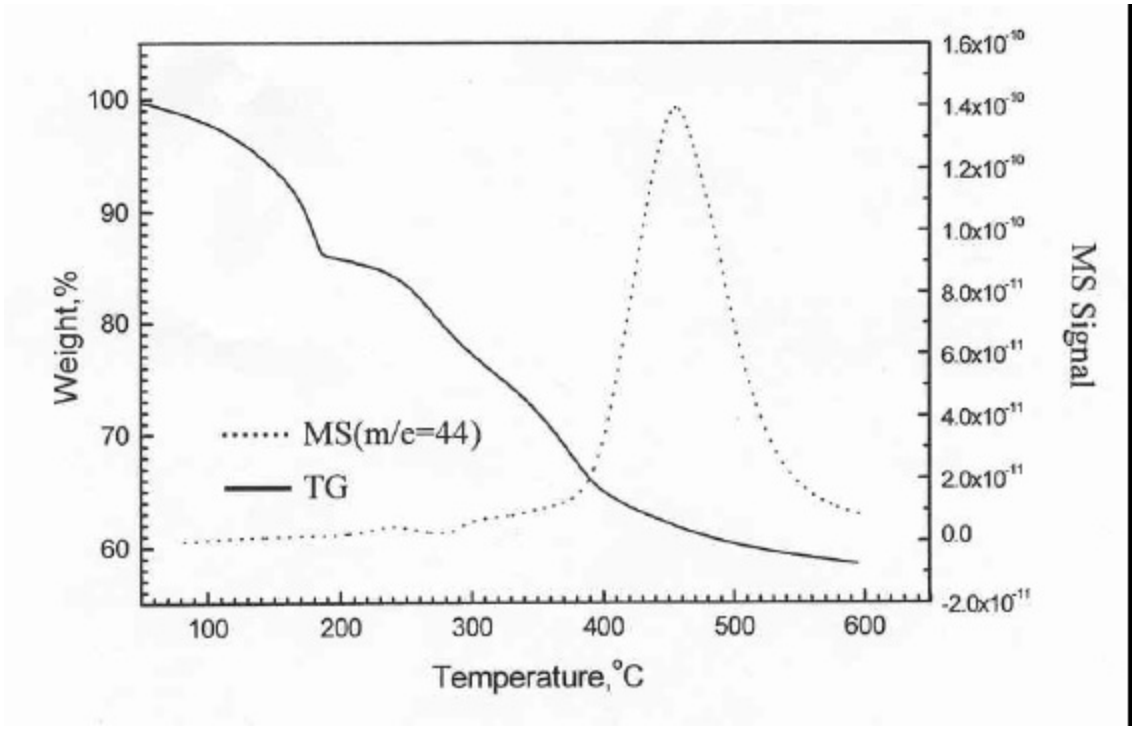

Figure 2.6 *In-situ* TG/MS of Mg-Al-CO_3 LDH as a function of temperature.

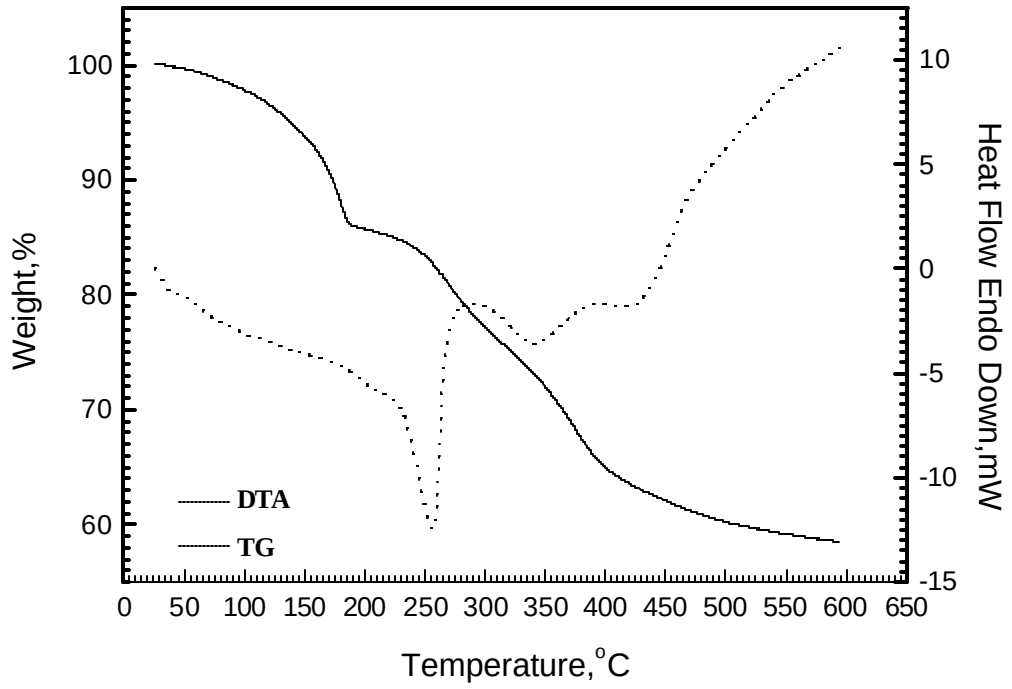

Figure 2.7 *In-situ* TG/DTA of Mg-Al-CO_3 LDH as a function of temperature.

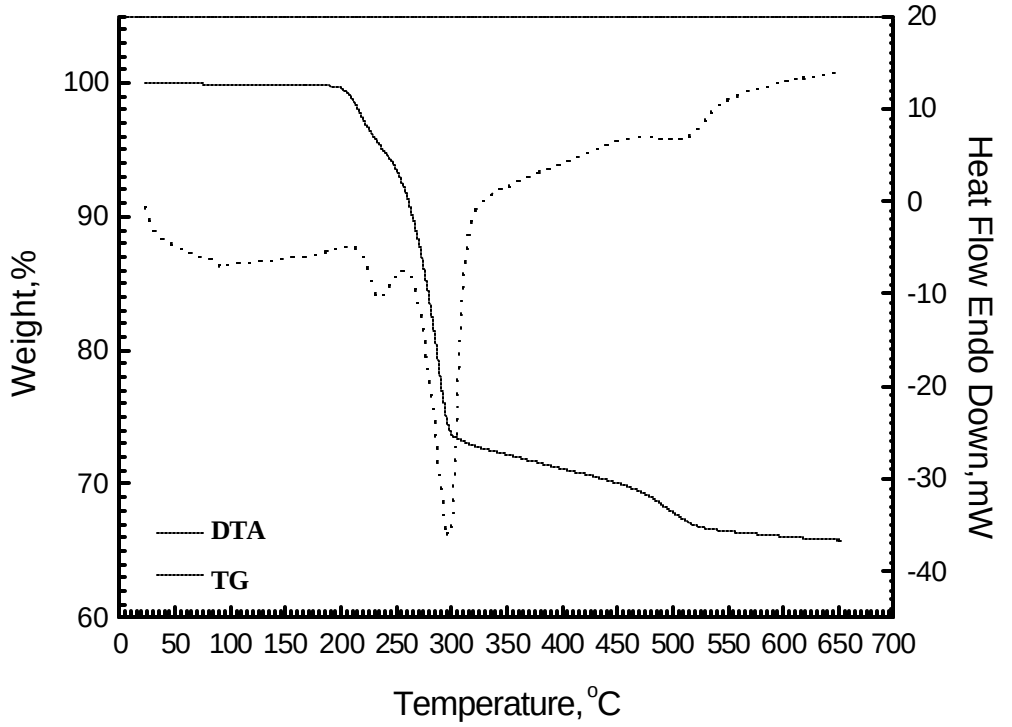

Figure 2.8 *In-situ* TG/DTA of $Al(OH)_3$ as a function of temperature.

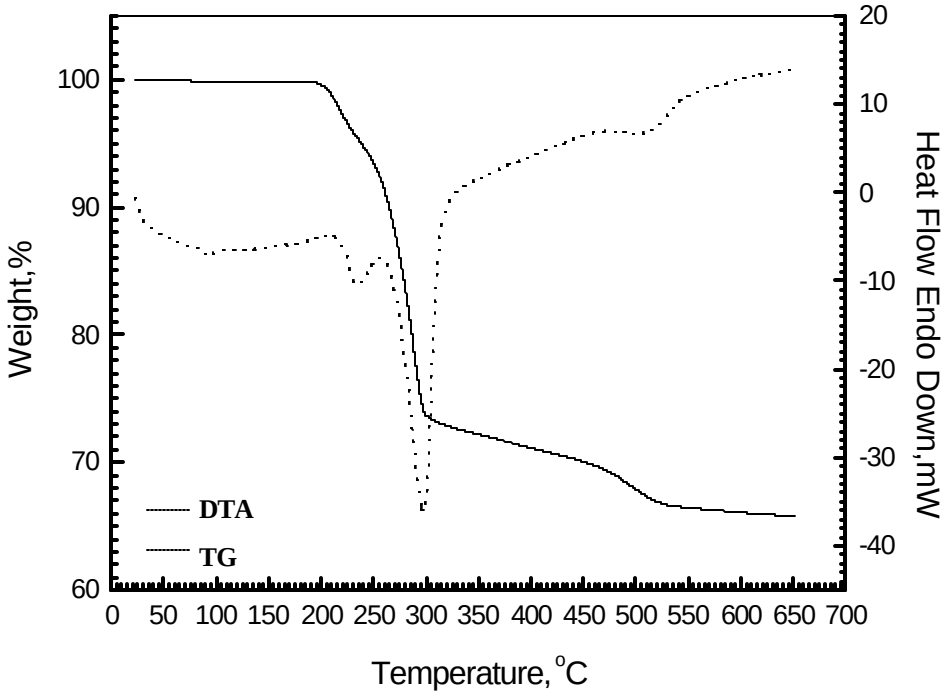

Figure 2.9 *In-situ* TG/DTA of $Mg(OH)_2$ as a function of temperature.

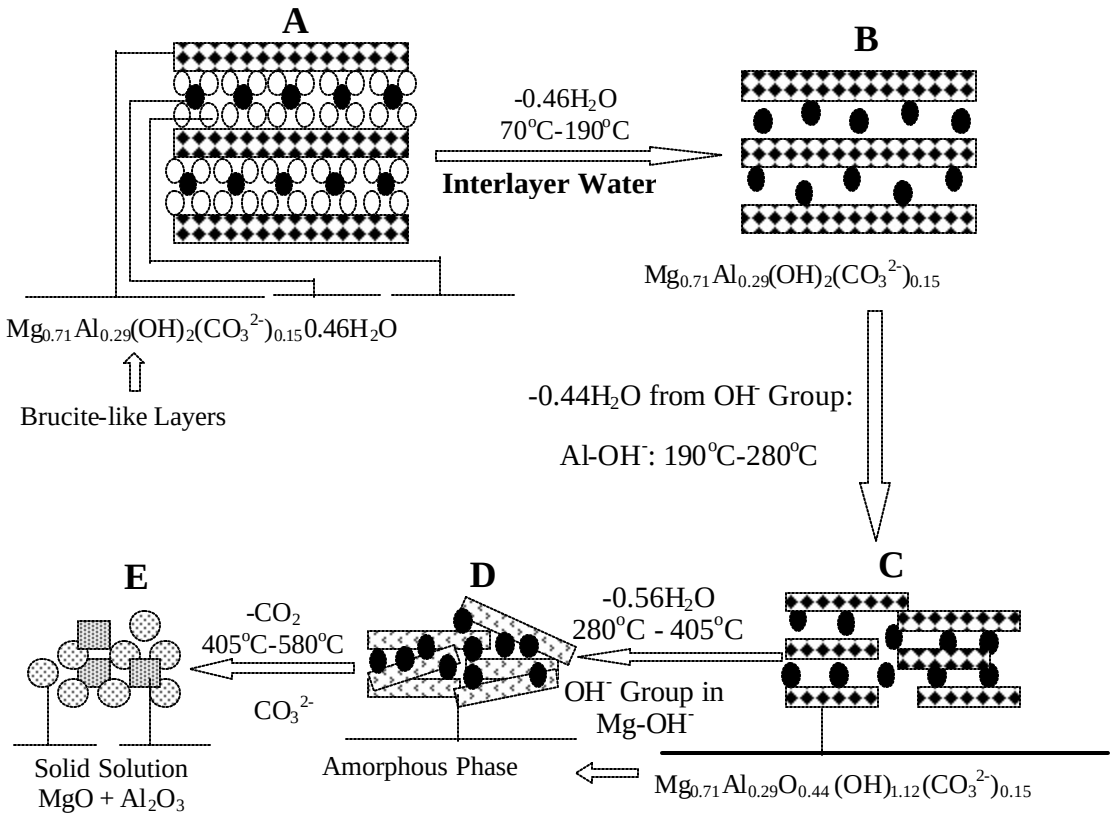

Figure 2.10 The thermal evolution of Mg-Al-CO_3 LDH as a function of temperature.

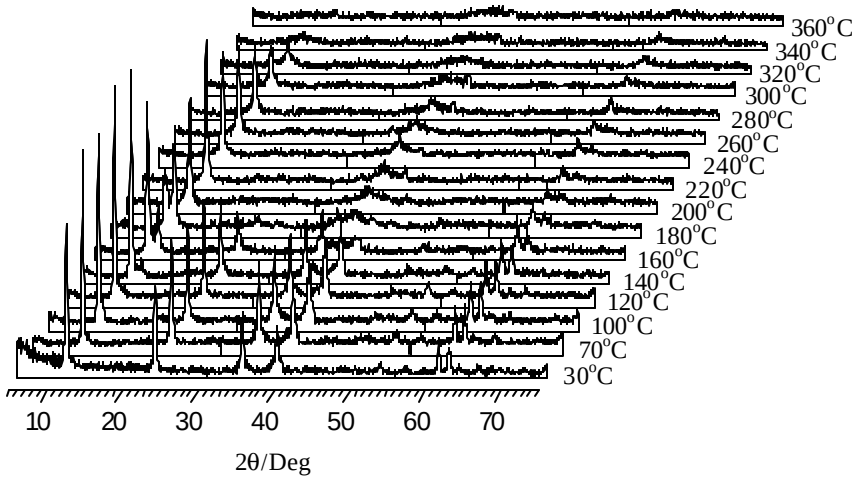

Figure 2.11 *In-situ* HTXRD of Mg-Al-CO_3 LDH as a function of temperature.

Chapter 3

CO_2 Affinity of Mg-Al-CO_3 LDHs and its Reversibility

3.1 Introduction

Thermal evolution pattern of the Mg-Al-CO_3 LDH material is discussed in the previous chapter. A notable feature of the Mg-Al-CO_3-LDH is its significant amount of CO_2 release at a higher temperature, indicating its CO_2 affinity. This chapter focuses on the study of the reversibility of the CO_2 affinity under both inert and reactive atmospheres. The reversibility of the CO_2 affinity under a reasonable industrial operating condition (i.e., in terms of temperature, pressure and atmosphere) is an essential property required for the formation of a commercially viable CO_2 adsorbent and membrane based upon the proposed LDH material.

3.2 Experimental

Material Characterization… The two LDH samples used in this chapter were represented by $Mg_{0.71}Al_{0.29}(OH)_2(CO_3)_{0.15}\cdot 0.46(H_2O)$ (LDH1; the same LDH sample utilized in previous chapter), and $Mg_{0.645}Al_{0.355}(OH)_2(CO_3)_{0.178}\cdot 0.105(H_2O)$ (hereinafter referred to as LDH2) based upon the analysis by ICP and TGA. These samples were characterized with the instrumentation described below:

- DRIFTS (Diffused Reflectance Infrared Founier Transform Spectroscopy) spectra vs temperature, pressure, and various atmospheres were recorded *in situ* using a Genesis II (Mattson, FT-IR) instrument equipped with a DRIFTS COLLECTOR™ II chamber (SpectraTech, Inc.) capable of operating under high temperatures (up to 900 ^oC) and pressures (up to 1500 psi). The experimental operating conditions were a DRIFTS scan-range from 4000 cm^{-1} to 500 cm^{-1}, scan numbers 16, and a scan resolution of 2 cm^{-1}.
- TGA curve was recorded with a Cahn TGA 121 instrument to determine the weight loss vs temperature. The MB-MS instrument is custom-made, using a MKS UTI 100C Precision Gas Analyzer.
- Surface analysis performed in this chapter includes SEM, TEM, and XRD. SEM images were taken with Cambridge Stereoscan 360, and TEM images were taken with Philips EM420 instrument. XRD figures were generated with Rigaku X-ray diffractometer.

The results obtained from the above analysis were used in this chapter to decipher the CO_2 reversibility of the Mg-Al-CO_3 LDHs and the operating condition required to achieve the reversibility.

Operating Condition for Adsorption/Desorption…We investigated, therefore, the ability of the LDH materials to reversibly adsorb CO_2 under a broad range of experimental

conditions. For each series of experiments, 100-120 mg of a fresh LDH sample was utilized. During the adsorption part of the cycle, 30 sccm of CO_2 was bubbled through a beaker containing distilled water (the CO_2 stream's RH being ~ 70%) and the sample was exposed to this humidified CO_2 stream for varying periods of time. Subsequently to adsorption, the flow of CO_2 was shut-down and the desorption part of the cycle was initiated. To find optimal experimental conditions for sorption studies, the effect of varying the duration of adsorption was investigated. And it was observed that increasing the time of adsorption from 1 to 2 hr increased the total amount adsorbed by about 5%, but a subsequent increase from 2 hr to 3 hr had no additional significant effect. Therefore, for the remainder of the study, an adsorption step time of 3 hr was utilized. Also two different methods to carry out the desorption step were investigated. In the first method, upon termination of the CO_2 flow, the sample was exposed to flowing UHP dry Ar at a rate of 30 sccm. Typically, after 30 min the weight change of the sample ceased. Subsequently, Ar was flowed to continue for a total desorption period of 1 hr. In the second method, the chamber was evacuated for a period of 1 hr at a pressure below 40 mTorr. Evacuation was shown to be a more effective means for carrying out the desorption step (~ a 10% increase in weight gain upon subsequent readsorption), and was adopted for the remainder of the study.

Reversibility via Pressure Swing... For each experiment, at any given temperature, a fresh LDH2 sample (100-120 mg) was used. The temperature was increased from room temperature at a rate of 5°C/min in an Are atmosphere (flow rate of 30 scum) to the preset point (e.g., 200°C, 250 °o, etc.), and kept at this temperature until the sample weight became constant, typically for 20~30 min. Subsequently, the cyclic sorption/adsorption experiments were initiated via the pressure swing. Multiple adsorption/adsorption cycles were then carried out at two selected temperatures, 150 and 250°C. Upon reaching the desired temperature, the feed was switched to humidified carbon dioxide (20 scums, 70% RH) and kept there for 3 hr. Then the sample was evacuated for 1 hr, switched back to humidified carbon dioxide for 3 hr, and so on. Upon completion of the 14 cycles at 150°C, the LDH1 sample was heated in UHP dry Are (20 scum; 5°C/min) until its temperature reached 250°C; the feed was then switched to humidified CO_2 (20 scum, 70% RH), and kept there for 3 hr. Then, the sample was evacuated for 1 hr, switched back on to humidified CO_2 for 3 hr, and so on.

Reversibility Study via Temperature Swing…After the cyclic sorption/adsorption experiments with the LDH samples were completed, a number of experiments were initiated in which the weight-gain/loss of the sample was monitored as its temperature was cycled from room temperature to a preset temperature, and back down to room temperature. The same LDH1 sample was used in all of temperature cycling experiments reported in this section. In the first experiment, the sample was heated in flowing Are (20 scum) with a heating rate of 3°C/min from room temperature to a temperature of 150°C; subsequently the flowing Ar feed was substituted with a humidified CO_2 feed (20 scum) and was cooled down to room temperature with a 3°C/min cooling rate. Upon reaching room temperature, the sample was kept at this temperature for an additional 2 hr. The weight-loss/gain data are shown in Figure 3.12. The total weight-loss for the LDH1 sample was ~5.5% at 150°C; upon cooling in the humidified CO_2 atmosphere, the sample

recovered 98.4% of its original weight. The gaseous components evolved during the heating step were monitored by mass spectrometry (Figure 3.13); only water was detected during the experiment.

Upon termination of the experiment at 150°C, the humidified CO_2 atmosphere was switched back to flowing UHP dry argon, and the temperature was slowly (3°C/min) increased to 200°C. Upon reaching this temperature, the same experimental protocol was followed. The weight-loss curve leveled-off after 240 min. The sample was then cooled to determine the percentage of weight recovered (Figure 3.12). The gases evolved during the heating part of the cycle were also monitored (Figure 3.14). Water was detected throughout the whole temperature range, and trace amounts of carbon dioxide were detected from 195°C ~ 200°C. Most of the weight loss was observed below 150°C; only ~0.2 % of the weight-loss was observed between 180 °o and 200 °o.

Upon completion of the experiment at 200°C, the humidified CO_2 atmosphere was switched back to dry argon, and the temperature was slowly (1°C/min) increased to 250°C (in the 250°C and higher temperature cycling experiments, the cooling/heating rates were changed from 3°C/min to 1°C/min). Upon reaching this temperature, the flowing Ar feed was substituted with a humidified CO_2 feed (20 scum), and the sample was cooled down to room temperature with a 1°C/min cooling rate. Also the sample was allowed to equilibrate at room temperature for as long as necessary for the weight-gain curve to level-off.

Reversibility Study at Increased Pressure…To further study the sorption reversibility behavior of the LDH at the water gas shift (WGS) membrane reactor environment, similar experiments were carried out using a moderate-pressure adsorption flow system. The experimental system was equipped with mass flow controllers and a flow control valve at the exit to maintain the system pressure constant under flow conditions. Two types of experiments were performed. In the first series of experiments the flow system was first pressurized with flowing dry argon (50 scum) to 50 psig , then the temperature was increased to 250 °C, using a 5 °C /min heating rate (it took ~ 45 min), and the system was kept at 250 °C for 1 hr as a adsorption step. When the adsorption step was over, the system was cooled down to 150°C (cooling rate 5°C/min, ~ 20 min) in flowing dry argon (50 scums). Subsequently, the inlet gas was changed to dry CO_2 (50 scum) from argon, while keeping the same pressure of 50 psig for 3 hr as an adsorption step. During the adsorption step, the outlet flow rate was monitored by a digital flow meter (while the reactor pressure was maintained constant at 50 psig), and, from the flow rate change, the amount of adsorption was calculated. Table 3.3 shows the weight gain during the sorption step for the first 3 sorption/adsorption cycles with the LDH2 sample.

In the second series of experiments the LDH2 sample (~ 14 g) was first heated to a preset temperature in Ar gas (50 scum). Each cycle involved first evacuating the sample for 1 hr as a desorption step. After the evacuation step, the flow system was then again pressurized to 50 psig in flowing Ar. When the outlet flow rate was stabilized in flowing Ar at 50 psig, the inlet gas was then changed to either dry or humidified CO_2 (50 sccm) for 3 hr while maintaining the same pressure of 50 psig. Upon completing the first

adsorption/desorption cycle the procedure was repeated for a number of additional cycles, and for a number of temperatures.

3.3 Results and Discussion

Characterization with TGA and XRD…The weight losses for the two LDHs were studied by TG-MS, and the results were shown to be consistent with the ICP results, as indicated in Table 3.1. The LDH2 sample has a higher Al/Mg ratio (the value of x being near the higher end of the typical LDH range), and contains less interlayer water. XRD characterization of these two LDH samples indicates that the materials have the typical LDH XRD spectra as shown in Figure 3.1[1-3], but the XRD spectrum of LDH2 is noisier than that ofLDH1, and not as strong as the spectrum of LDH1 (compare Figure 3.1a with Fig 3.1b). The TGA spectra for the two LDHs generated with a scan rate of 5^oC/min, and the corresponding *in-situ* MS signals of CO_2 are shown in Figure 3.3a. The cumulative amounts of H_2O evolved are shown in Figure 3.3b. Though differences in the TGA and mass evolution spectra exist, the thermal evolution profiles of the two LDH's are about similar, only the ranges of temperatures for each peak are slightly different. Hibino *et* al[4] also observed differences in the TGA spectra of Mg-Al-CO_3-LDH with a different Al:Mg ratios, but even between LDH with the same Al:Mg ratio and different crystallite sizes[4]. For the LDH2, the loosely-held interlayer water is lost in the temperature range of 80 - 190^oC, the OH^- group begins to disappear at 190^oC and is completely lost around 520^oC. While some CO_3^{2-} loss is observed at lower temperatures, its substantial loss begins at 450 ^oC, and is completed at 720 ^oC. The fractions in terms of the total of H_2O and CO_2 evolved in different temperature ranges for both LDH1 and LDH2 are shown in Table 3.2. In summary, based upon the results of the thermal analysis and the XRD patterns, the two HT samples show typical hydrotalcite behaviors.

Table 3.1 Weight-loss from the TG/MB-MS studies, and calculated weight-loss based on the ICP data for the samples. (a) LDH1; and (b) LDH2.

(a)

Weight-Loss	H_2O	OH^- from Al	OH^- from Mg	CO_2 from CO_3^{2-}	Total Weight-Loss %
ICP Value	10.8%	10.4%	13.2%	7.2%	41.6%
Experimental from TG/MS	12.93%	8.93%	12.65%	7.72%	42.23%

(b)

Weight-Loss	H_2O	OH^- from Al	OH^- from Mg	CO_2 from CO_3^{2-}	Total Weight-Loss %

ICP Value	2%	11.0%	16.1%	10.9%	40%
Experimental from TG/MS	2%	12.08%	15.94%	11.06%	41.08%

Effect of Heating Rate and Atmosphere on Thermal Evolution Pattern…Up to 250 ^{o} C, heating rates up to 10C/min show no effect on the TGA curves; most likely the thermal evaluation behaviors are within the equilibrium, not the kinetic, control. However, >250°C, some of the heating rates effects are apparent and likely the thermal evaluation behavior is within the kinetic control. Similar observations were previously made by Costantino and Pinnavaia[5], and most recently by Rhee and Kang[6]. To investigate the effect of heating rate further, the weight-loss characteristics of the LDH2 sample have been studied for 4 different heating rates, namely, 1, 3, 5 and 10^{o}C/min, and in three different atmospheres. The weight-loss results in an inert Ar atmosphere and the corresponding MS signals of CO_2 are shown in Figure 3.4a. For the results in Figure 3.4, a fresh LDH2 sample ~110-120 mg was used in every experiment, and dry inert Ar (ultra high purity grade) was utilized as a purge gas at a flow rate of 20 sccm. For heating rates below 5 ^{o}C/min the weight-loss curves and the MS signals coincide, indicating that the structural changes (loss of interlayer water, hydroxyl, and CO_3^{2-} losses) occur rapidly enough, so that the LDH structure equilibrates within the time frame allotted by the changing temperature. However, the results with the 10 ^{o}C/min heating rate show kinetic effect in comparison with the lower heating rate results. Similar observations were also made in the presence of dry and humid CO_2 atmospheres, with the results showing absence of kinetic effects for heating rates below 5 ^{o}C/min.

Table 3.2 The fractions of H_2O and CO_2 (as % of the total sample weight) that are evolved in different temperature ranges for both LDH1 and LDH2.

	LDH1			LDH2		
	Weight-Loss, %	H_2O	CO_2	Weight-Loss, %	H_2O	CO_2
RT~100^{o}C	2.61	2.61	-	0.59	0.59	-
100~200^{o}C	11.39	11.31	0.08	1.48	1.46	0.02
200~300^{o}C	8.03	7.94	0.09	7.41	7.33	0.08
300~400^{o}C	12.64	11.95	0.69	8.31	8.04	0.27
400~500^{o}C	4.8	0.7	4.1	10.42	9.91	0.51
500~600^{o}C	2.76	-	2.76	11.38	2.69	8.69
600~750^{o}C	-	-	-	1.49	-	1.49
Total	42.23	34.51	7.72	41.08	30.02	11.06

The effect of varying the heating rate on weight-loss for the LDH2 sample was also studied in the presence of a reactive atmosphere. For the experiments in Figure 3.4b, in addition to the weight-loss of the LDH2 sample in the presence of inert Ar, we also show

the weight-loss curve for the case in which dry CO_2, instead of Ar, was utilized as a purge gas atmosphere at a flow rate of 20 mL/min and a heating rate of 5°C/min. The weight-loss results in the presence of a humidified CO_2 atmosphere are also shown in the same figure. Measurements of the water concentration of the gas exiting the beaker indicate that the relative humidity (RH) of the CO_2 stream was ~ 70%. The results in Figure 3.3b indicate little effect of the gaseous atmosphere on the weight-loss curve in the first region of temperatures associated with the evolution of interlayer water. Differences exist, however, in the other regions. In the region where mostly CO_2 evolves, DRIFTS indicates that all hydroxyls in the LDH structure have already disappeared, the weight-loss curves for the humidified and dry CO_2 atmospheres coincide, but are still different from the weight-loss curve under inert conditions; the presence of CO_2 in the purge atmosphere appears to slow-down somewhat the rate of CO_2 evolution. The dry and humidified CO_2 weight-loss curves are different in the region associated with hydroxyl evolution, particularly in the range of temperatures associated with loss of hydroxyls in an Mg-(OH)-Mg configuration. Previously, Ding and Alpay[7], who studied CO_2 adsorption on a K-promoted commercial Mg-Al hydrotalcite at 400 °C, noted a small (~ 10%) beneficial effect of the presence of water on CO_2 adsorption. They also noted, however, that the actual partial water pressure did not really matter, with even traces of water vapor being capable of providing the same beneficial effect. Ding and Alpay[7] attributed this beneficial effect to the ability of water vapor to either maintain the hydroxyl concentration on the surface or to prevent the sites from poisoning through carbonate or coke deposition. In summary, heating rate of 5°C/min or less shows no kinetic effect, which was adopted in the later study. In addition, the presence of CO_2 in the desorption atmosphere appears slow down the desorption process as expected.

CO_2 Reversibility via Pressure Swing…The ability of the LDH to reversibly adsorb CO_2 and H_2O is of significance in the use of these materials as adsorbents and membranes. In the former case, the ability to reversibly adsorb CO_2 is critical from the standpoint of being able to regenerate the adsorbent via pressure swing; in the latter case the presence of a relatively mobile CO_2 phase within the LDH structure is beneficial to the permeation of CO_2 through the membrane as a pressure driven process. The adsorption/desorption behavior of the LDH2 at selected temperatures ranging from 150 to 350°C was performed. Figure 3.5a shows the total weight gain (as percent fraction of the original weight of the LDH sample) during the adsorption part of the cycle. Figure 3.5b shows the corresponding total weight-loss during the desorption part of the cycle. Figure 3.5c presents the weight change of individual components, H_2O and CO_2, during the desorption part of the cycle.

Three distinct regions can be distinguished in Figure 3.5c. The first region is for temperatures below 190°C, in which the LDH2 sample reversibly adsorbed only water and slight amounts of CO_2. The cyclic adsorption/desorption results indicate that the exchange of interlayer water is a fairly reversible process. In the second temperature range, from 190°C to 280°C, water from the hydroxyl groups that are bonded with Al cations releases. In addition, some CO_2 is also emitted in this region. After the initial sorption/desorption cycle, however, only CO_2 appears to be reversibly adsorbed in this

region, with very little H_2O emitted; the sample weight change can be fully attributed to the reversibly adsorbed CO_2.

In the temperature range of 280 – 440 ^oC, the previous studies indicate that the OH^- group bonded with Mg^{2+} begins to disappear at 280^{o}C, and is completely lost at 440 ^oC (for the LDH2 the upper temperature extends higher – see Table 3.2). Degradation of the hydrotalcite structure is also observed in the same region. Again, after the initiation of the sorption/desorption cycle, however, only CO_2 appears to be reversibly adsorbed in this region, with very little H_2O emitted. Hence, the sample weight change can be mostly attributed to the reversibly adsorbed CO_2. As can be seen in Fig 3.5c, the amount of CO_2 that is reversibly adsorbed in this region decreases as the temperature increases, consistent with the observations that the crystallinity of the hydrotalcite material also decreases, and its structure begins to fall apart in this region.

To further validate the cyclic sorption/desorption behavior, *in situ* cyclic flow sorption/desorption experiments using the DRIFTS system were carried out, following the same experimental protocol as with TG/MB-MS experiments described above. Figure 3.5 presents the DRIFTS spectra with temperature as a parameter. Figure 3.6b shows the peak area representing the CO_3^{2-}, ν_3, vibration during the cyclic adsorption/ desorption experiments[1]. Figure 3.6c shows the peak area representing 3470 cm^{-1} band corresponding to the OH^- vibration, and the combined peak areas for the interlayer water peaks (3070 cm^{-1} and 1620 cm^{-1})[1]. In Figure 3.6b and 3.6c it was observed that at 150^{o}C only the combined peak area representing the interlayer water changed in a reversible manner. No substantial changes are observed through the adsorption/ desorption cycles in the peak areas reflecting the CO_3^{2-},ν_3, vibration or the 3470 cm^{-1} band corresponding to the OH^- vibration. According to the above observations, the hydrotalcite exchanges reversibly the interlayer water at temperature <150°C. At a higher temperature, i.e., >150°C, after the initial adsorption/desorption cycle, the hydrotalcite exchanges reversibly only CO_2. These observations are consistent with the TG-MS experiments and the observations of previous chapter.

Multiple cyclic adsorption/desorption experiments were also performed. Figure 3.7 shows the weight change and the residual weight (both as percent fraction of the original sample weight) observed for a total of 14 cycles. Figure 3.8 shows the corresponding MS signals during the heating and evacuation part of the cycle. The system reaches a steady-state reversible behavior after the 11th cycle, with the corresponding weight change being 0.23%.

Figure 3.9 shows the weight change observed for a total of 14 cycles for the LDH1 sample at 250 ^oC. The sample reaches a steady state behavior after the 9th cycle, with the corresponding reversible weight change being 0.31%. Figure 3.10 shows the corresponding MS signals during the heating and evacuation parts of the cycle. Figure 3.11 describes a long-term cycling experiment using 113 mg of LDH2 at 250 ^oC, following the same other experimental conditions as with the experiments involving the LDH1 sample. The sample reaches a steady state behavior after the 14th cycle, with the corresponding reversible weight change being 0.32%. In summary, ~0.3% reversible and

steady CO_2 capacity was observed, implying the permeation of CO_2 with LDH-based membrane via the CO_2 pressure drop can be accomplished.

CO2 Reversibility via Temperature Swing… In addition to pressure swing, temperature swing was also considered by us as a means to demonstrate the reversibility although temperature swing was rarely practiced. Upon cooling from 250 to 25°C, 99.2% of original weight of the sample was recovered as shown in Figure 3.15. The components evolved during the heating part of the cycle were also monitored (Figure 3.16). Water was detected throughout the whole temperature range, similar to the previous experiments, and smaller amounts of carbon dioxide were detected in the range from 195 - 250°C. The experiment was repeated with the temperature raised (1°C/min) to 300°C, cooled down in humidified CO_2 to room temperature. As shown in Figure 3.15, it took a much longer time than in the previous experiments for the sample to re-gain the weight, which leveled off at 96% of original weight. The composition of outlet gas showed water evolution through the whole range of temperatures; carbon dioxide was again detected between 195 and 300°C. The experimental results with the temperature raised to 350°C are also shown in Figure 3.15. Once more, it took a much longer time for the sample to recover its weight, which leveled off at 93.8% of its original weight; water was evolved through the whole region of temperatures and carbon dioxide was detected between 195 and 350°C. The CO_2 reversibility was demonstrated via the temperature swing from 150 – 350°C to room temperature, consistent with the results from pressure swing with temperature as a parameter.

Study of Reversibility at Increased Pressure…The reversibility property was further studied here under a moderate pressure, i.e., 50 psig, in reference to the use of these materials for the low temperature water gas shift (WGS) reaction. Similar experiments were carried out using a moderate-pressure adsorption flow system.

Table 3.3 Weight-gain during the sorption step for the moderate-pressure flow experiments using dry CO_2.

	Weight-gain during the adsorption step (wt. %)
1st Cycle	2.621
2nd Cycle	2.542
3rd Cycle	2.476

Table 3.4 Weight-gain during the adsorption step for the moderate pressure flow experiments at various temperatures using dry CO_2.

	150°C	200°C	250°C
1st Cycle	2.02	1.84	1.72
2nd Cycle	1.97	1.79	1.69
3rd Cycle	1.87	1.71	1.68
4th Cycle	1.84	1.69	1.66

Table 3.5 Weight-gain during the sorption step for the moderate pressure flow experiments at various temperatures using humidified CO_2.

200 °C	Weight gain at adsorption step (wt. %)
1st Cycle	1.85
2nd Cycle	1.79
3rd Cycle	1.73
4th Cycle	1.71

The cyclic adsorption/desorption results for the various temperatures for dry CO_2 are summarized in Table 3.4, while those for humidified CO_2 for one temperature are shown in Table 3.5 (a fresh LDH2 sample was utilized for each set experiments at every new temperature). For the experiments in Table 3.5, the CO_2 stream contains 2% mol of water, which corresponds approximately to 70% RH at the temperature and pressure of the experiment. Again, at 150°C, the weight loss during the desorption part was attributed to the release of water with trace CO_2. Opposite to the run at 150°C, the runs at 200 and 250°C released primarily CO_2. Comparing between the run in humidified CO_2 (Table 3.5) and dry CO_2, little difference was observed in the weight change, which was consistent with the observation under atmospheric conditions. In summary, the CO_2 reversibility under moderate pressure conditions is in agreement with the TG/MB-MS and DRIFTS data under atmospheric conditions. The effect of water appears insignificant for the temperature and pressure range we studied.

3.4 Conclusions

The thermal evolution of CO_2 under atmospheric and moderate pressure conditions is in agreement with the LDH structural model suggested in the previous chapter. The LDHs are shown capable of CO_2 exchanging reversibly for a broad region of conditions. These experimental observations qualify the LDH as base material for the formation of CO_2 permselective membranes and CO_2-affinity adsorbents for high temperature membrane reactor applications as proposed in this project. The ability to reversibly adsorb CO_2 is critical from the standpoint of being able to regenerate the adsorbents. The presence of a relatively mobile CO_2 phase within the LDH structure is important in determining the

permeation rate through the membrane. The CO_2 capacity and its transport rate as an adsorbent, as well as the permeability and selectivity as a membrane, were experimentally determined which are presented in Chapter 4&6

Literature Cited

1. Kanezaki, E. Effect of atomic ratio Mg/Al in layers of Mg and Al layered double hydroxide on thermal stability of hydrotalcite-like layered structure by means of *in-situ* high temperature powder X-ray diffraction. *Mater. Res. Bull.,* 1998, *33(5),* 773.
2. Kanezaki, E. Thermal behavior of the hydrotalcite-like layered structure of Mg and Al-layered double hydroxides with interlayer carbonate by means of *in-situ* powder HTXRD and DTA/TG. *Solid State Ionics,* 1998, *106(3-4),* 279.
3. Cavini, F.; Trifiro, E.; Vaccari, A. Hydrotalcite-type anionic clays – preparation, properties and applications. *Catal. Today,* 1991, *11,* 173.
4. Hibino, T.; Yamashita, Y.; Kosuge, K.; Tsunashima, A. Decarbonation behavior of Mg-Al-CO_3 hydrotalcite-like compounds during heat treatment. *Clays and Clay Minerals,* 1995, *43(4),* 427.
5. Constantino, V. R. L.; Pinnavaia, T. J. Basic properties of $Mg_{1-X}(2+)Al_X(3+)$ layered double hydroxides intercalated by carbonate, hydroxide, chloride, and sulfate anions, *Inorg. Chem.,* 1995, *34*, 883.
6. Rhee, S. W.; Kang M. J. Kinetics on dehydration reaction during thermal treatment of Al-CO3-LDHs, *Kor. J. Chem. Eng.,* 2002, *19*, 653.
7. Ding, Y.; Alpay, E. Equilibria and kinetics of CO_2 adsorption on hydrotalcite adsorbent. *Chem. Eng. Sci.,* 2000, *55,* 3461.

(a)

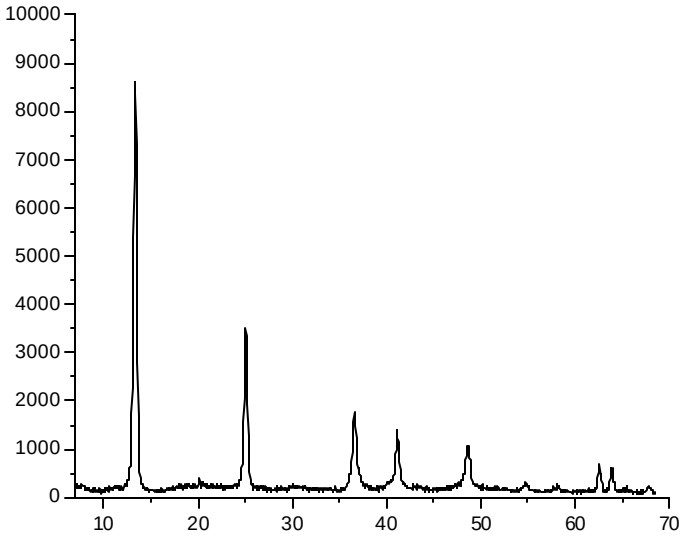

(b)

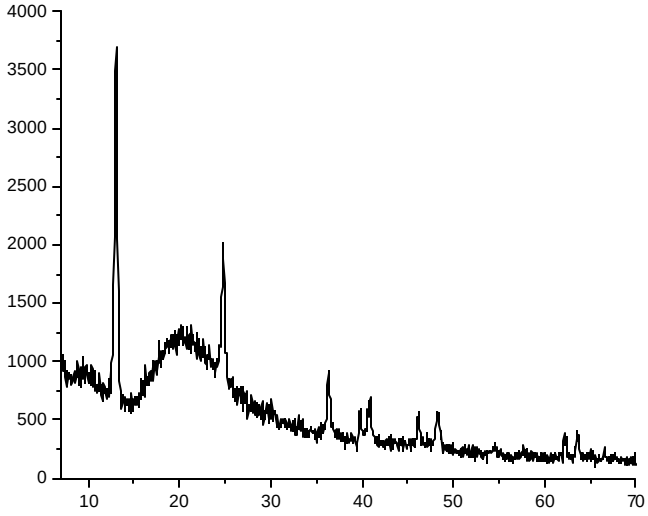

Figure 3.1 The XRD spectra of the LDH samples (a) LDH1 sample; (b) LDH2 sample.

(a)

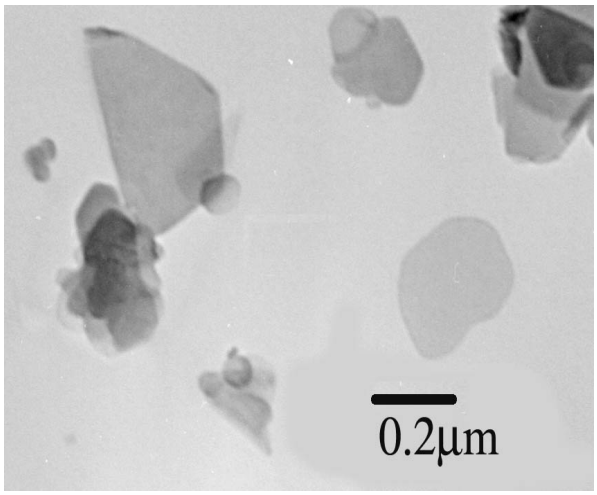

(b)

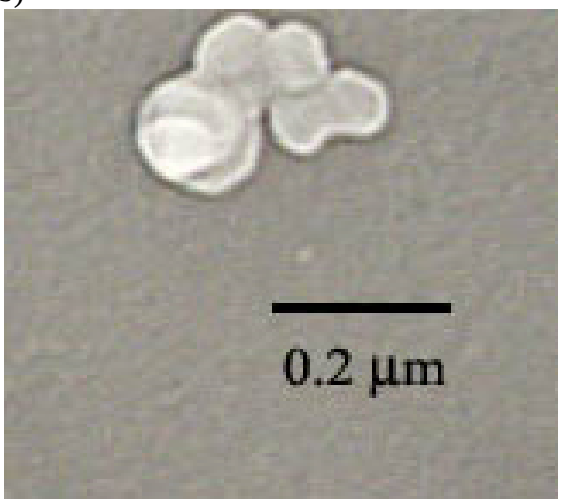

Figure 3.2 (a) TEM picture of LDH1; (b) TEM picture of LDH2.

(a)

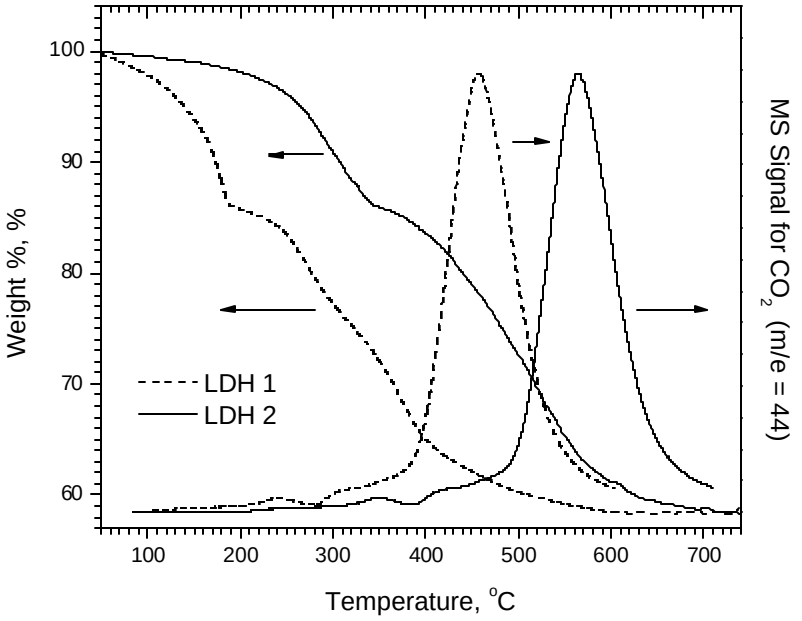

(b)

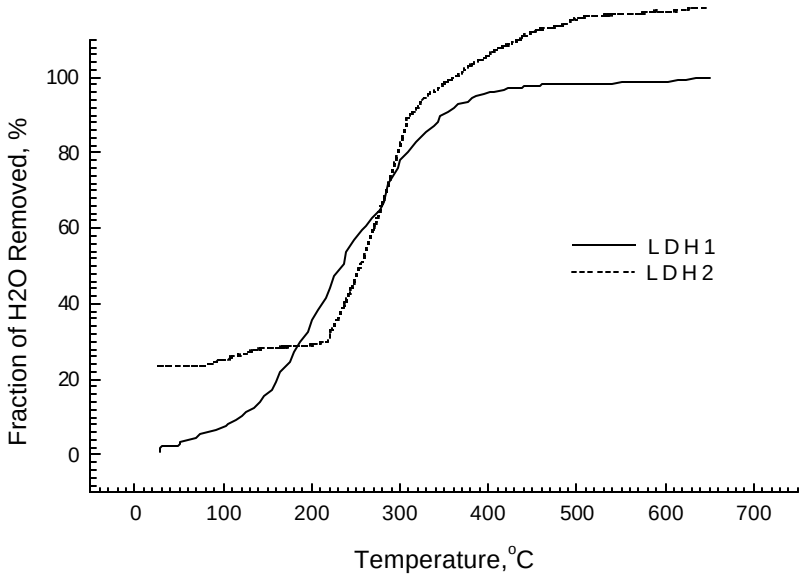

Figure 3.3 The TGA spectra and CO_2 MS signal for the two LDH samples generated with a scan rate of 5°C/min; (b) cumulative amount of H_2O evolved.

(a)

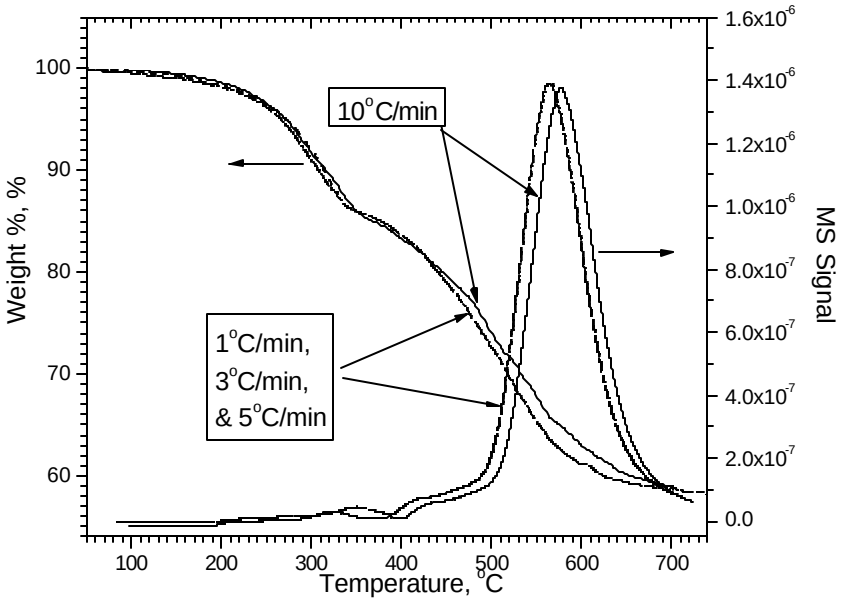

(b)

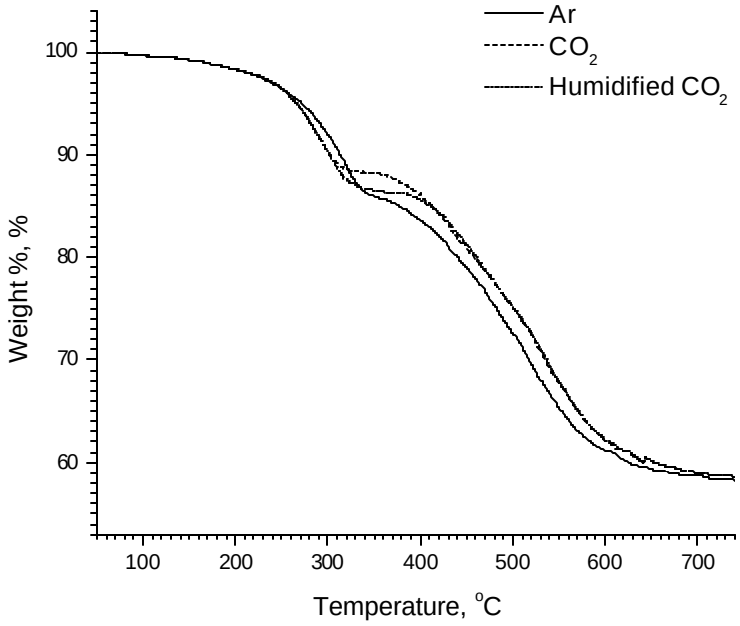

Figure 3.4 The effect of varying (a) the heating rate; and (b) of using different purging gases on the weight-loss for the LDH2 sample.

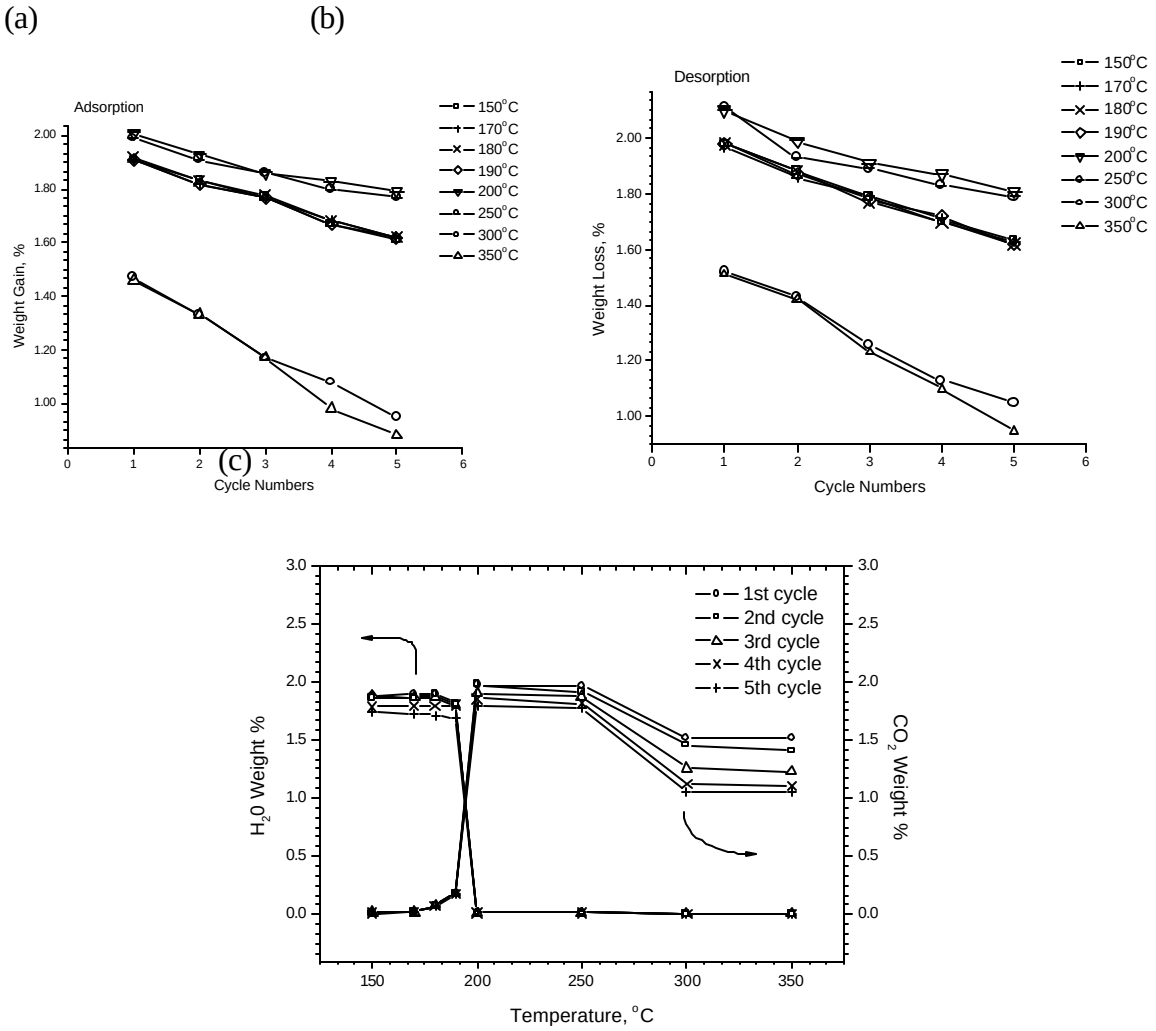

Figure 3.5 Weight-gain or loss. (a) weight-gain during adsorption for various temperatures as a function of the cycle number; (b) weight-loss during desorption for various temperatures as a function of the cycle number; (c) weight-change due to loss of water or CO_2 during desorption as a function of temperature.

(a)

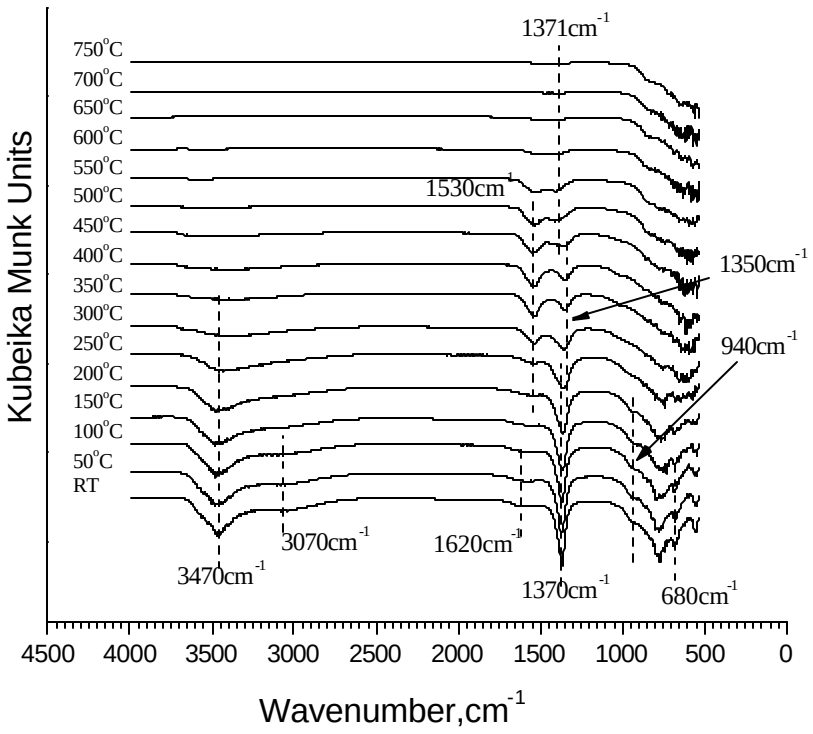

(b)

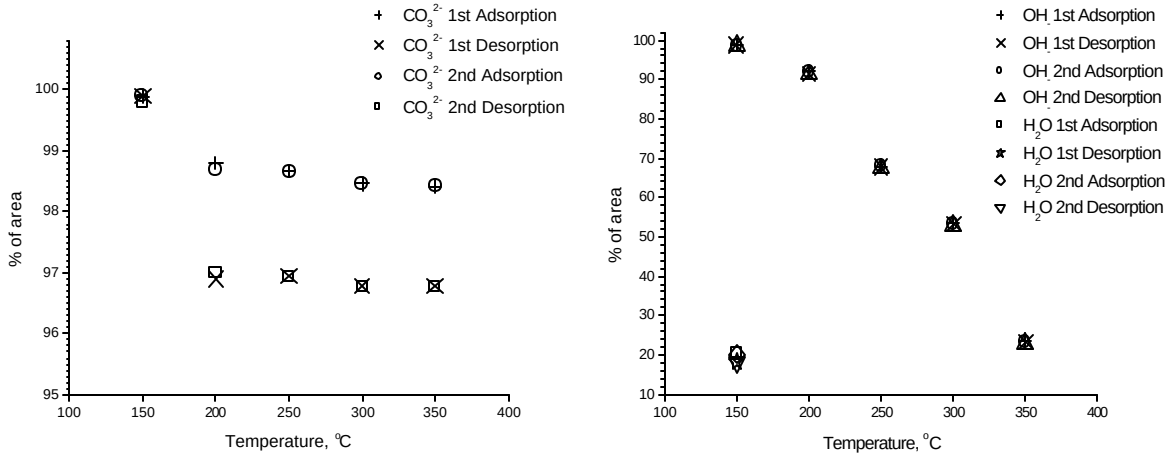

Figure 3.6 (a) *In-situ* DRIFTS of LDH2 as a function of temperature; (b) change in the CO_3^{2-} integrated peak area (left), and change in the OH^- and H_2O integrated peak areas as a per cent fraction of the original peak area (right) during the sorption/desorption cycles.

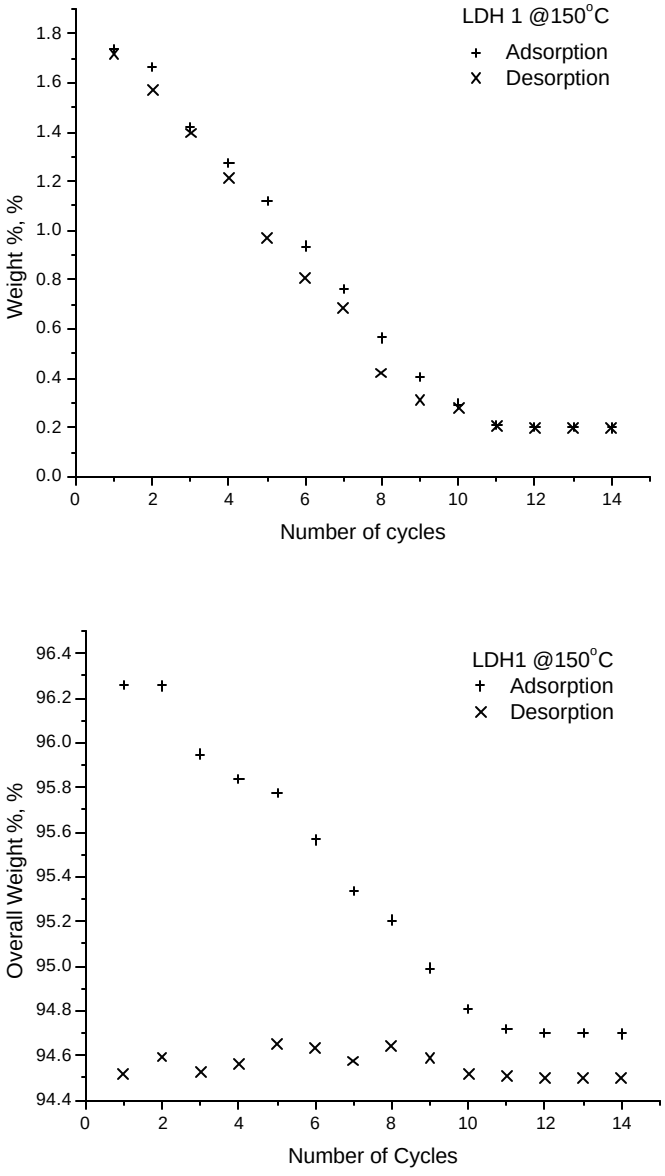

Figure 3.7 Weight-gain or loss (top) and total sample weight (bottom) during the sorption/desorption cycles.

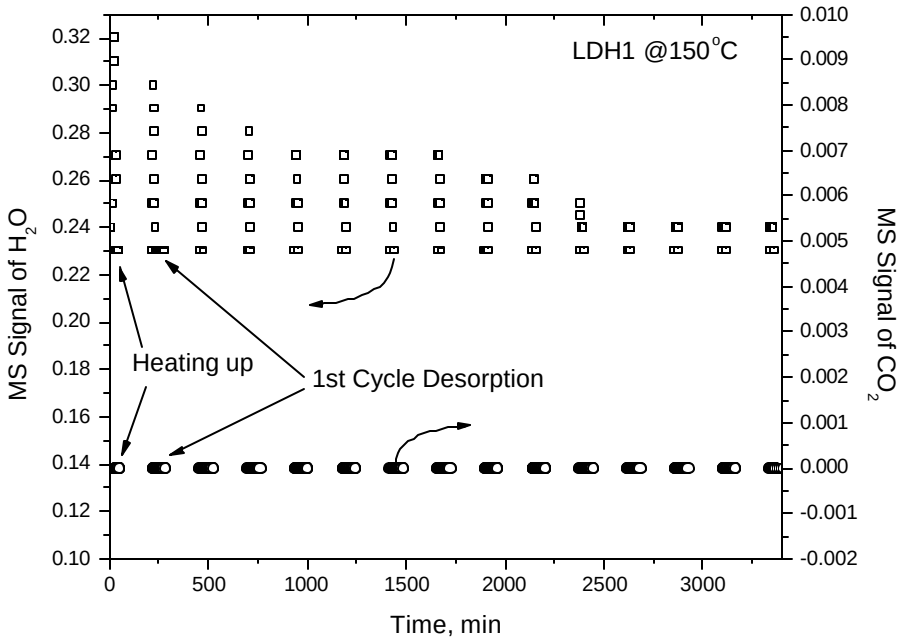

Figure 3.8 H_2O and CO_2 MS signals during the heating, and the desorption part of the cycles as a function of time.

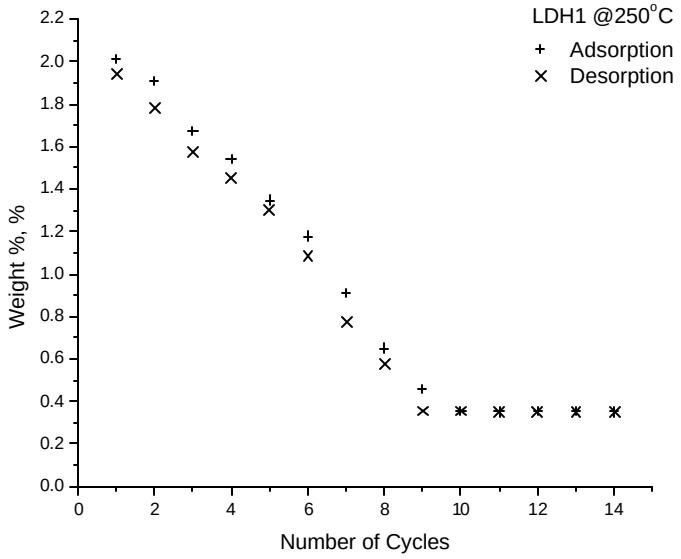

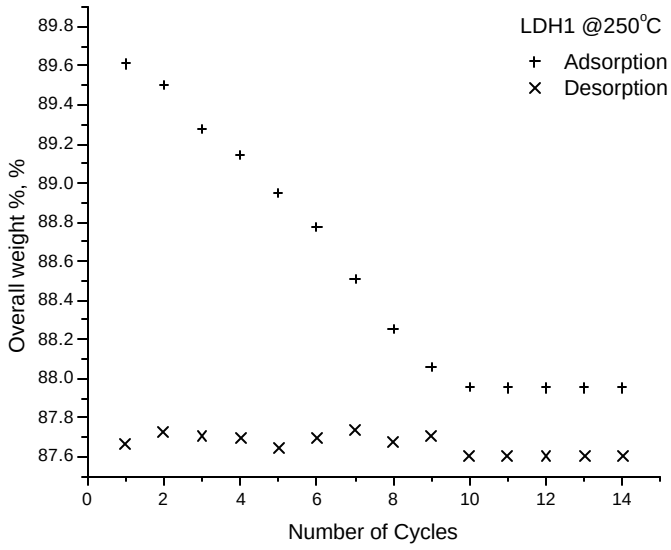

Figure 3.9 Weight-gain or loss (top) and total sample weight (bottom) during the sorption/desorption cycles.

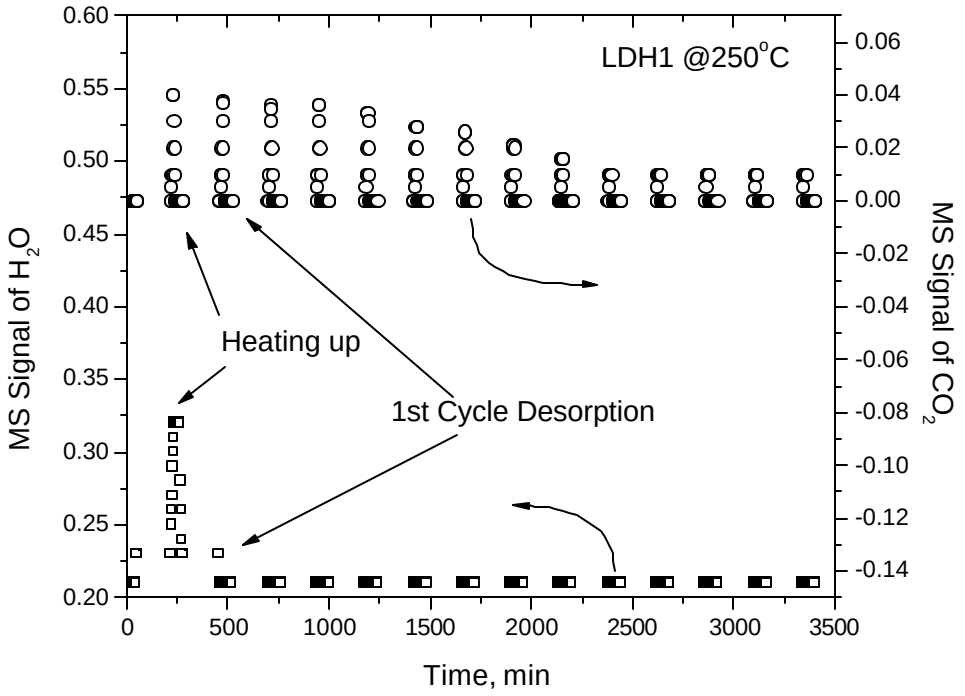

Figure 3.10 H_2O and CO_2 MS signals during the heating, and the desorption parts of the cycle as a function of time.

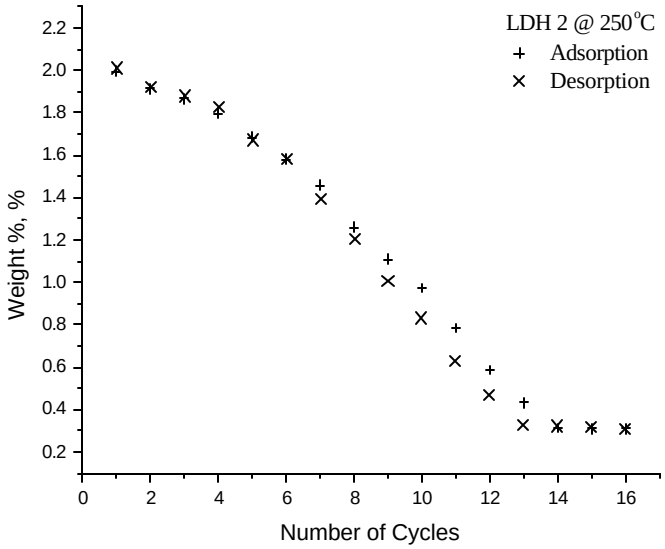

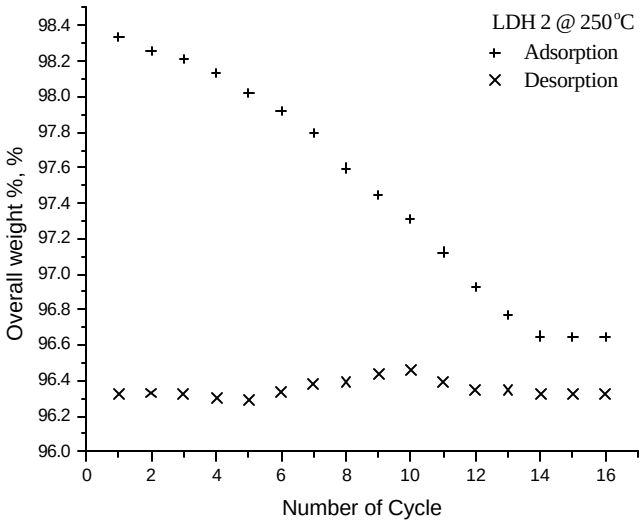

Figure 3.11 Weight-gain or loss (top) and total sample weight (bottom) during the sorption/desorption cycles.

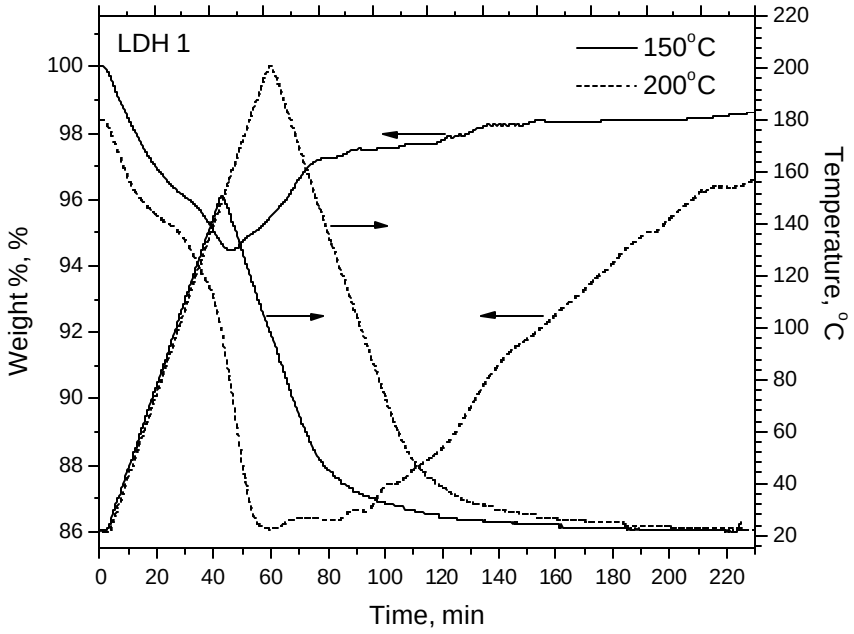

Figure 3.12 Weight-loss/gain during the temperature cycling experiments. Solid lines are the experiments from room temperature to 150°C; Dotted lines are experiments from room temperature to 200°C.

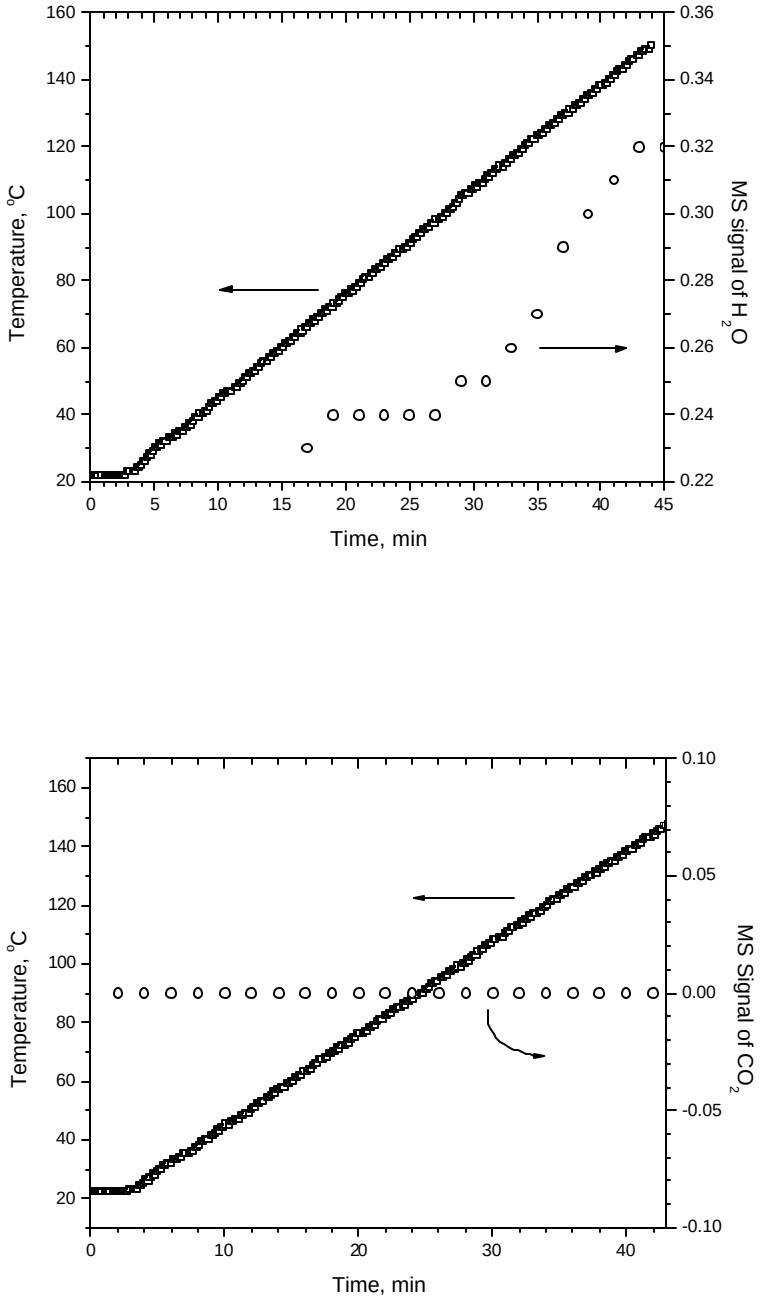

Figure 3.13 MS signals for H_2O (top) and CO_2 (bottom) during the temperature cycling experiment from room temperature to 150°C.

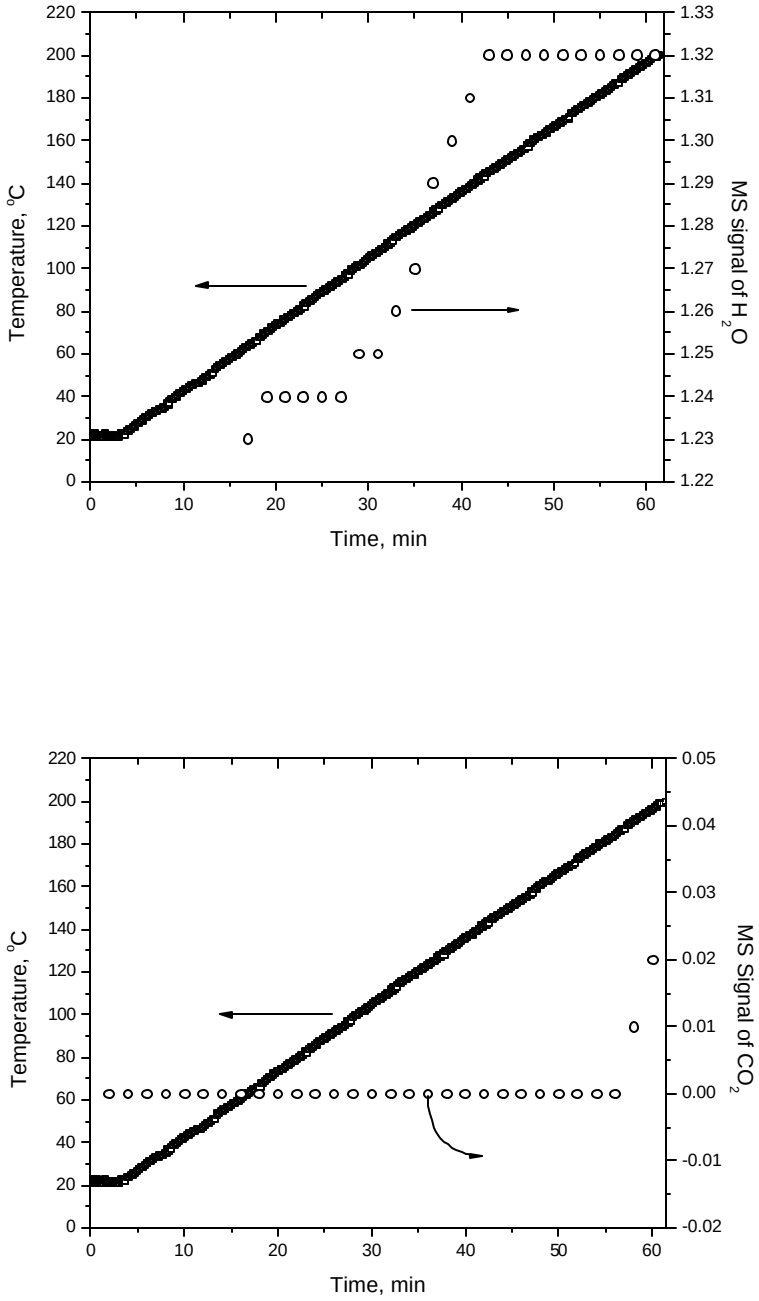

Figure 3.14 MS signals for H_2O (top) and CO_2 (bottom) during the temperature cycling experiment from room temperature to 200°C.

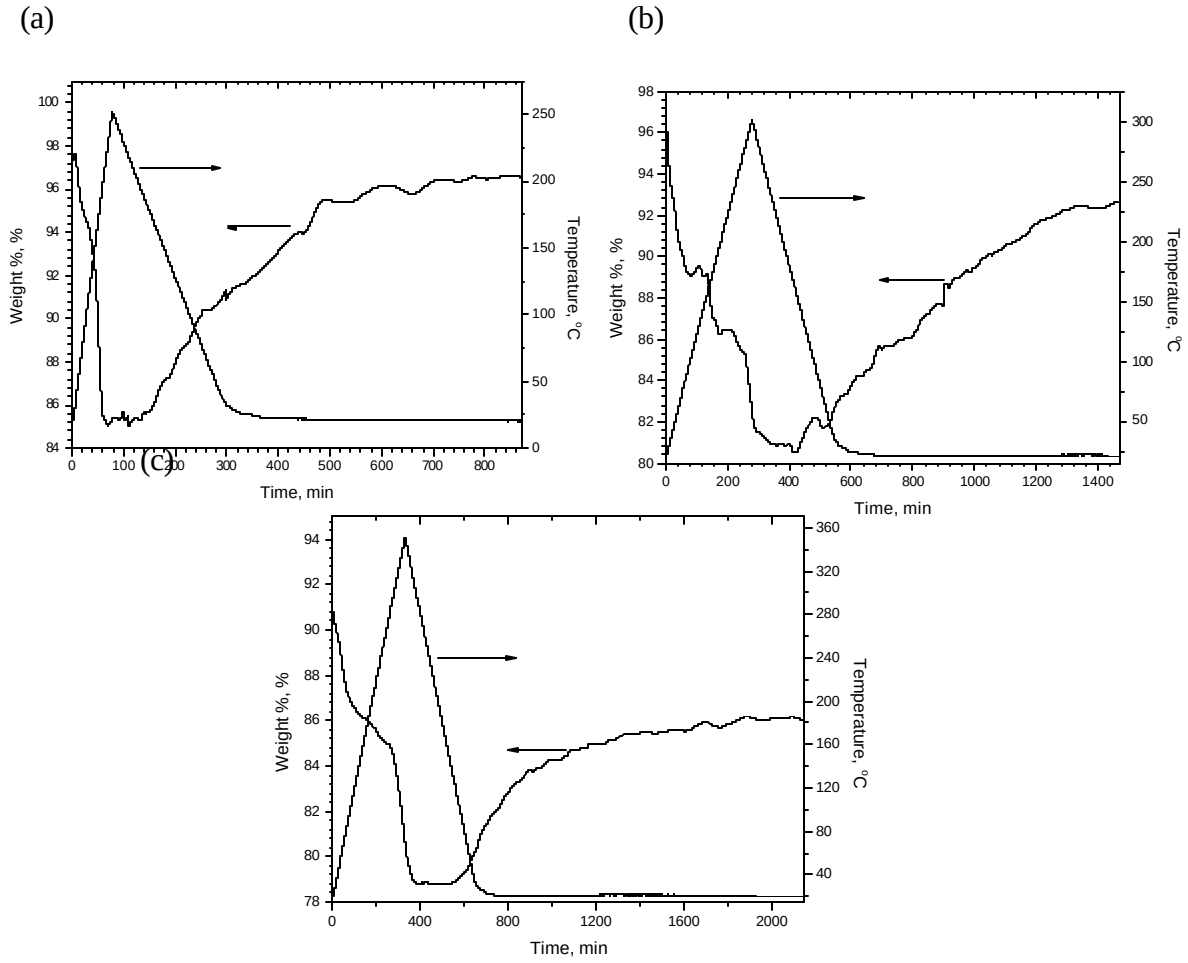

Figure 3.15 Weight-loss/gain during the temperature cycling experiments (a) from room temperature to 250°C; (b) from room temperature to 300°C; (c) from room temperature to 350°C.

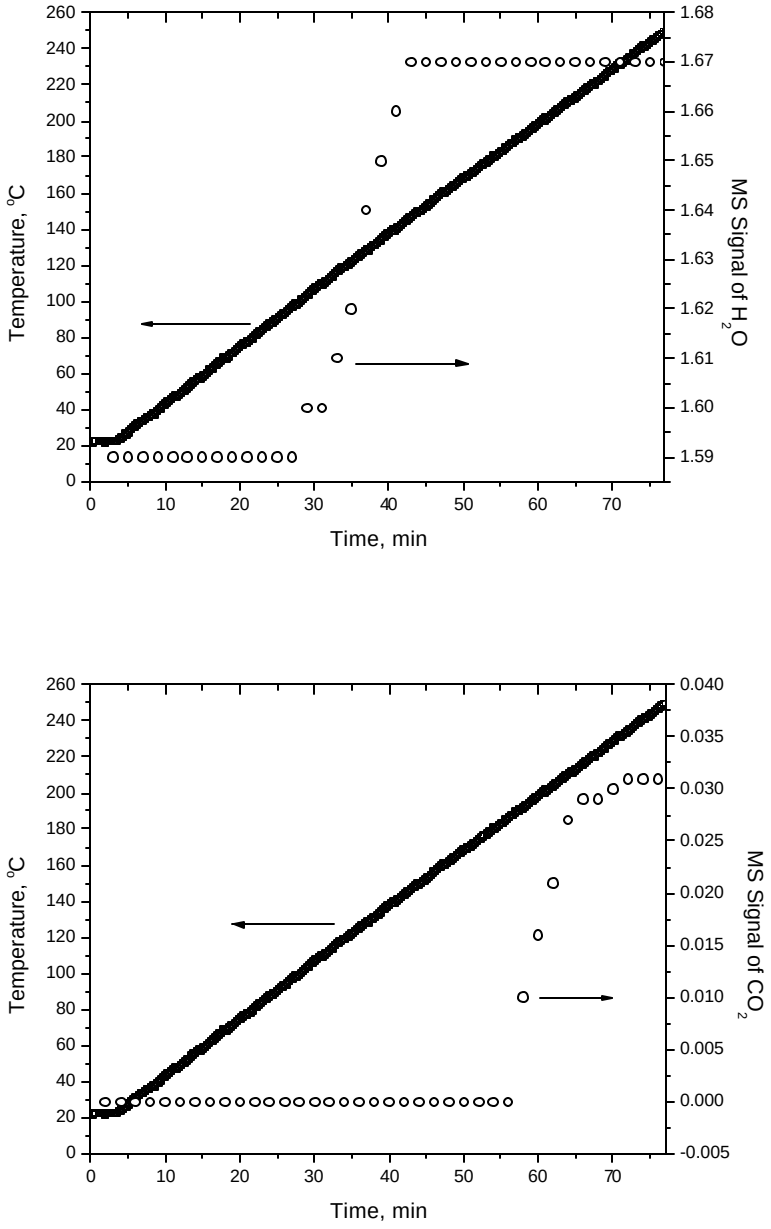

Figure 3.16 MS signals for H_2O (top) and CO_2 (bottom) during the temperature cycling experiment from room temperature to 250°C.

Chapter 4

Synthesis and Characterization of CO_2 Affinity Membrane with LDH Material

4.1 Introduction

Based upon its CO_2 reversibility presented in Chapter 3, the LDH material could form an ideal CO_2 semipermeable membrane (see conceptual schematic in Figure 4.1) if a thin and defect free LDH film can be deposited on porous substrate. This chapter focuses on the synthesis aspect of the LDH membrane undertaken in this project. Two different methods were attempted for the preparation of the LDH membrane. They are (i) in-situ crystallization, and (ii) slip casting. In addition, chemical vapor deposition/infiltration (CVD/I) was also investigated for back patching the synthesized LDH membranes. Our experience on each method is summarized in this chapter along with the results, discussions and recommendations for future study.

4.2 Hydrotalcite Membrane Formation via In-situ Crystallization

Our previous study suggested the possibility that hydrotalcite crystals in the neighborhood of 0.2μm or greater are immediately formed when the two precursor reagents (i.e., Na_2CO_3 and $AlCl_3/MgCl_2$) are combined together. The conventional approach (such as methods developed for the zeolitic membrane) involving the deposition of pre-formed crystals as seeds for crystal growth within the porous structure of the membrane becomes unnecessary. It is feasible to form a single crystal of hydrotalcite within the membrane porous structure if the two reagents can be combined together within the porous structure of substrate. This rationale represents a major advantage for membrane synthesis, which can eliminate many tedious steps in the crystal formation as in the zeolitic membrane development. A two-phase contactor using the membrane as an interphase appears to be an ideal device for us to achieve in-situ crystal formation within the porous structure of the membrane. To demonstrate feasibility, a batch type two phase contactor was used to simplify the equipment design, acquisition and set-up.

4.2.1 Experimental

- *Approch*…To deposit hydrotalcite into the porous structure of the ceramic substrate as described in Figure 4.2, we proposed the interphase contact approach. It was hoped that the precipitate could be deposited within the porous structure to form constriction with hydrotalcite crystals. Detailed procedures are described below:

    a. In the beginning, we filled the tube side of a membrane (plugged at one end *a prior* with one of the reactants, $AlCl_3/MgCl_2$), thereby completely wetting the pores of the substrate with the reactant. Then, the tube was dipped into a batch of

well-mixed Na_2CO_3 solution. This approach was designed to embed hydrotalcite crystals in the pores of the support near the outer tubular surface because the two solutions in contact at the membrane surface are stagnant and do not intermix rapidly.

b. Three porous ceramic membranes with 40Å, 500Å and 0.2μm pore sizes (available commercially from Media and Process Technology Inc.) were selected as candidate substrates for this study. Each tubular membrane was 10" long, 5.5mm OD and 3.5mm ID; one end was plugged with epoxy to hold the $AlCl_3/MgCl_2$ solution.

c. The tube was left in the batch solution for 0.5 to 1 hour to assure complete crystal formation. Then the tube was withdrawn and thoroughly rinsed with water and then dried. As part of the feasibility study, this crystal formation step was repeated up to 4 times to study the degree of crystal embedding/coverage. Thus 4 samples were generated for each pore size.

d. The experimental condition we selected was pH=10 to form the precipitate in-situ. Then, the impregnated membrane was autoclaved at 150ºC for 4 hours to insure the transformation of the precipitate into hydrotalcite crystals. Although our results indicated the formation of crystals even without autoclaving, we performed autoclaving for the time being to eliminate the uncertainty associated with this parameter. Several trials were performed for the preparation of the membranes via impregnation. Between each impregnation, the membrane is subject to autoclaving, water rinsing, and drying.

- *Characterization*…The permeance of the membrane after impregnation was used as an index for the degree of pore plugging of the starting membrane. Generally the above procedure was repeated for 2 to 4 times to reduce the nitrogen permeance of the membrane to <1-3 $m^3/m^2/hr/bar$ for post treatment by CVD to plug the residual opening/defects. In this section, three membranes were selected representing the starting membrane after 1st, 2nd and 4th layer of the in-situ crystallization step. These membranes were characterized by (i) He and N_2 permeance at room temperature, (ii) pore size distribution with a flow-weighted pore condensation porometer, and (iii) SEM.

4.2.2 Results and Discussions

- Evidently the hydrotalcite crystal was formed within the porous structure of the a-Al_2O_3 substrate with 0.05 and 0.2μm pore size based upon (i) the significant reduction in permeance of He and N_2 as shown in Table 4.1, (ii) the increase in the selectivity of He/N_2 (Table 4.1), (iii) the reduction in the pore size and/or pore volume (see Figure 4.4), and (iv) XRD spectrum of the hydrotalcite membrane (see Figure 4.15). As expected, the pore size reduction for the 0.05μm membrane was substantial after the 4th deposition. The increase in selectivity and reduction in

permeance are supportive of the pore size reduction by the in-situ formation of the hydrotalcite crystal.

- SEM photomicrographs of the inner and outer tubular surface of the 0.2µm membrane after in-situ crystal formation are presented in Figure 4.5. No plugging of the inner surface of the membrane was observed. The pore plugging was clearly shown in the outer tubular surface under both low (top, Figure 4.5) and high magnification (bottom, Figure 4.5). EDX mapping shown in Figure 4.6 confirms the formation of the presence of hydrotalcite crystals.

- The penetration of the crystal is believed to be very limited, since the microporous structure of the cross section of the membrane did not exhibit any deposition even near the outer tubular surface (see Figure 4.5). On the other hand, crystal spill-over to the top of the outer tubular surface is believed to be minimal because the surface topography of the substrate still visible as indicated by the absence of Mg in these areas (see Figure 4.7). Thus, the morphological evidence indicates that the proposed synthesis protocol delivers an ultrathin hydrotalcite patch within the pores very near the surface of the substrate with little or no excess crystal formation on the surface via the proposed synthesis protocol.

- Again, a similar result was obtained with the 500Å substrate shown in Figure 4.8. The pore size reduction in this case was reduced dramatically by the crystals (see Figure 4.4) because of the large reduction in gas permeability of the membrane shown in Table 4.1.

- Repeated additional depositions of the hydrotalcite crystals further reduced the permeance and pore size (see Table 4.7). It is believed that the additional depositions resulted in further infiltration of the residual pore openings remained due to incomplete or non-uniform coverage from previous depositions. However, the majority of the crystals were embedded in the substrate during the 1^{st} deposition cycle based upon the dramatic permeance reduction after the first cycle.

- It appears that hydrotalcite does not cover the substrate completely based upon the SEM pictures of the top surface as shown in Figures 4.9 to 4.12 corresponding to the 1^{st}, 2^{nd}, and 4^{th} impregnation. Evidently the permeance levels off after the 4^{th} impregnation, more importantly, 85% permeance was reduced. However, the selectivity after the 4^{th} impregnation remains low, around Knudsen separation, indicating that defects exist. Further the SEM photograph after the 4^{th} impregnation (shown in Figures 4.11 & 4.12) is consistent with our speculation that defects remain. It appears that the defect shown in Figures 4.11 & 4.12 is resulted from the incomplete coverage left from the in-situ impregnation. The defect in the dimension of about 0.2 micron is not covered by the precipitate, most likely resulted from the lack of the reagents filled into this gap (for example an air pocket), during impregnation, and then no precipitate would form within the gap. The other possibility is that the membrane layer cracked after drying.

- Due to larger defects present in the membranes deposited on the 0.2 and 0.05 µm substrate, we then attempted to deposit hydrotalcite on the 40Å substrate. Figure 4.13 presents the SEM and EDAX profiles of the hydrotalcite membrane thus deposited. Permeances vs no. of layer deposition presented in Table 4.2 and Figure 4.3 indicate that >~90% permeance flux reduction was achieved after the 3rd layer of deposition. The selectivity of He/N_2 was enhanced to near or slightly above Knudsen selectivity, indicating that the deposition may have covered defects and possibly reduced the pore size of the starting membrane. The pore size distribution of the membrane after 4th deposition was compared with that of the starting membrane as shown in Figure 4.14. It appears that nearly all the pore size available from the substrate was covered with hydrotalcite. However, based upon its resultant selectivity in the neighborhood of Knudsen selectivity, defects remain dominant although the defect sizes are much smaller in this case.

Table 4.1: Permeance and Selectivity of the 500Å and 0.2µm Pore Size Ceramic Substrates Following In-situ Deposition/Crystal Growth of Hydrotalcite within the Pores. Based Upon the SEM Analysis, Crystal Growth is Concentrated at the Surface of the Membrane.

Pore Size of Substrate [µm]	Times of Deposition [-]	Permeance [$m^3/m^2/hr/bar$] @ 25°C		Ideal Selectivity [-]	Remarks
		Helium	Nitrogen		
0.05	0	81.2	41.5	1.96	control
0.05	1	2.04	0.913	2.24	
0.05	2	-	-	-	
0.05	3	5.22	2.35	2.22	
0.2	0	113	66.3	1.70	control
0.2	1	18.8	11.2	1.68	
0.2	2	-	-	-	
0.2	3	15.0	6.52	2.30	

Table 4.2 Permeance of Hydrotalcite Membranes prepared via 1st, 2nd and 3rd In-Situ Crystalization Step using 40Å Al_2O_3 Membranes as Starting Membranes

Sample ID	No. of Crystalization	Permeance (m3/m2/hr/bar) He	N2	Selectivity (He/N2)	
40A, typical		~60	~30	~2	
HT-IA-60-6	1st	23.34	8.93	2.61	
HT-IA-40-4	1st	28.57	11.47	2.49	
	2nd	13.98	6.19	2.26	
HT-IA-40-5	1st	16.93	6.67	2.54	
	2nd	8.75	3.19	2.74	
	3rd	8.47	3.24	2.61	?????
Knudsen, theoretical				2.65	

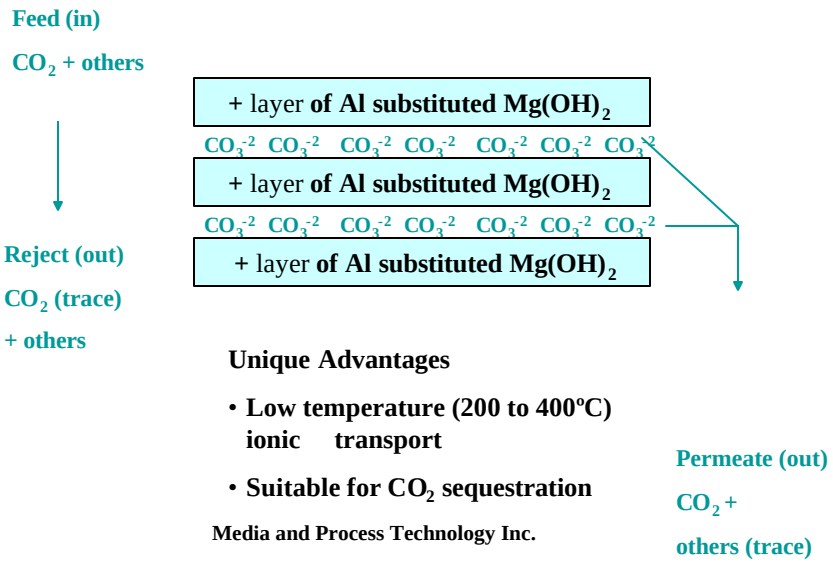

Figure 4.1 Affinity Ceramic Membrane with 2-D Transport Channel for CO_2

STEP	PURPOSE
1. Interphase contact of reactants	Formation of precipitates as precursors
2. Aging via autoclaving	Enhancing crystal stability and crystallinity
3. Rinsing	Removing impurities

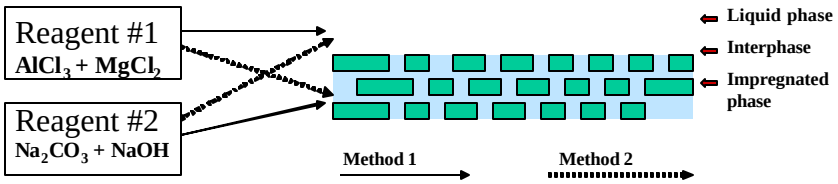

Figure 4.2 Hydrotalcite Membrane Synthesis via Impregnation

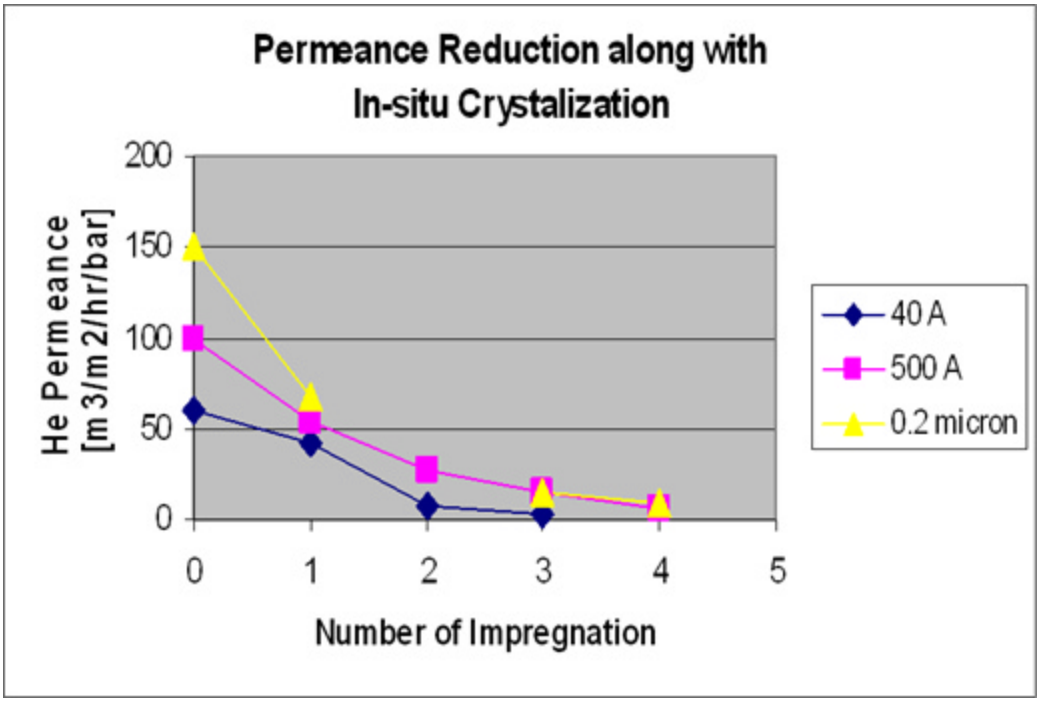

Figure 4.3 Permeance reduction along with number of in-situ crystallization for substrates with pore sizes of 40Å, 500Å and 0.2 µm

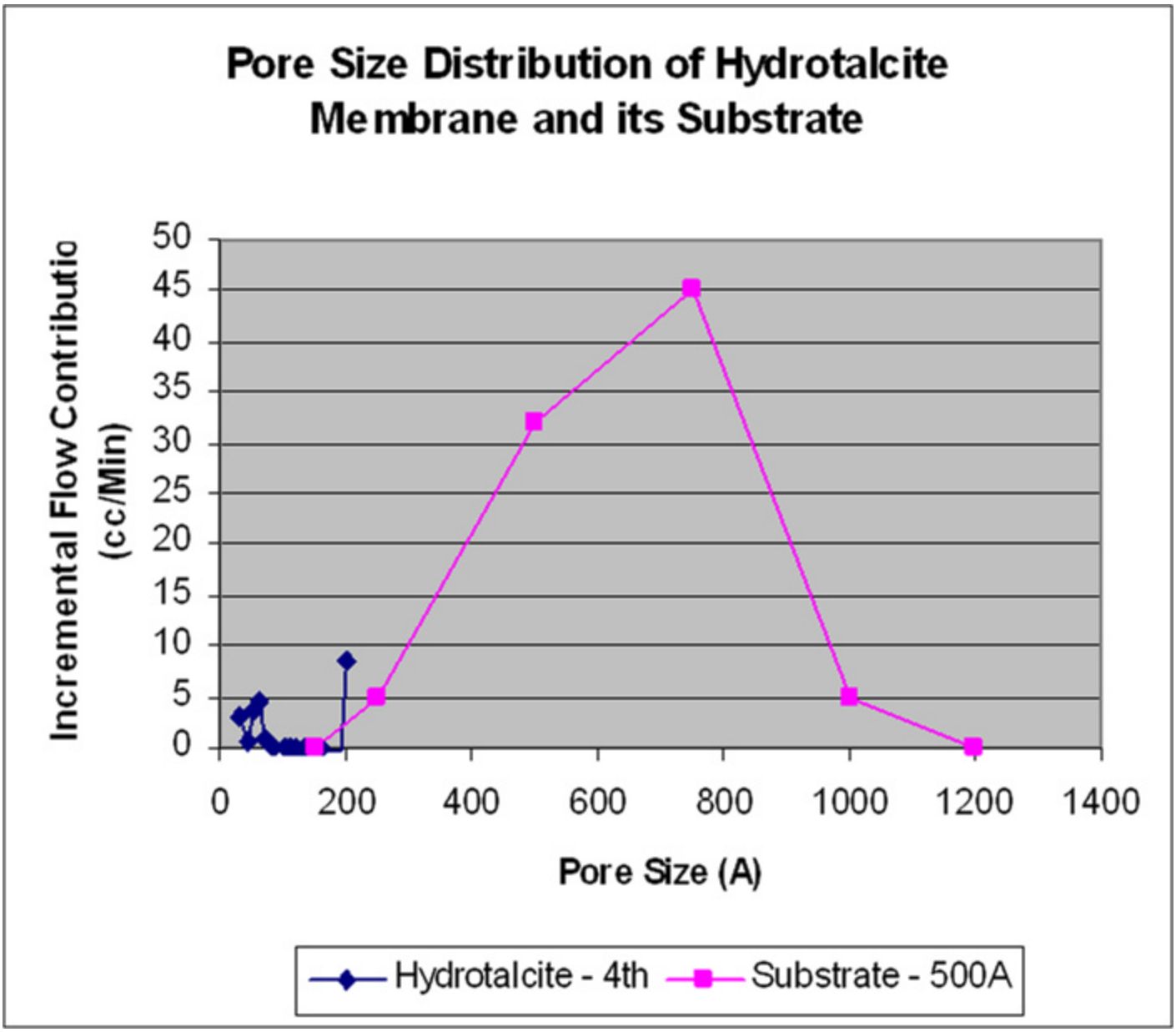

Figure 4.4 Pore size distribution of hydrotalcite membrane and its substrate with 500Å pore size.

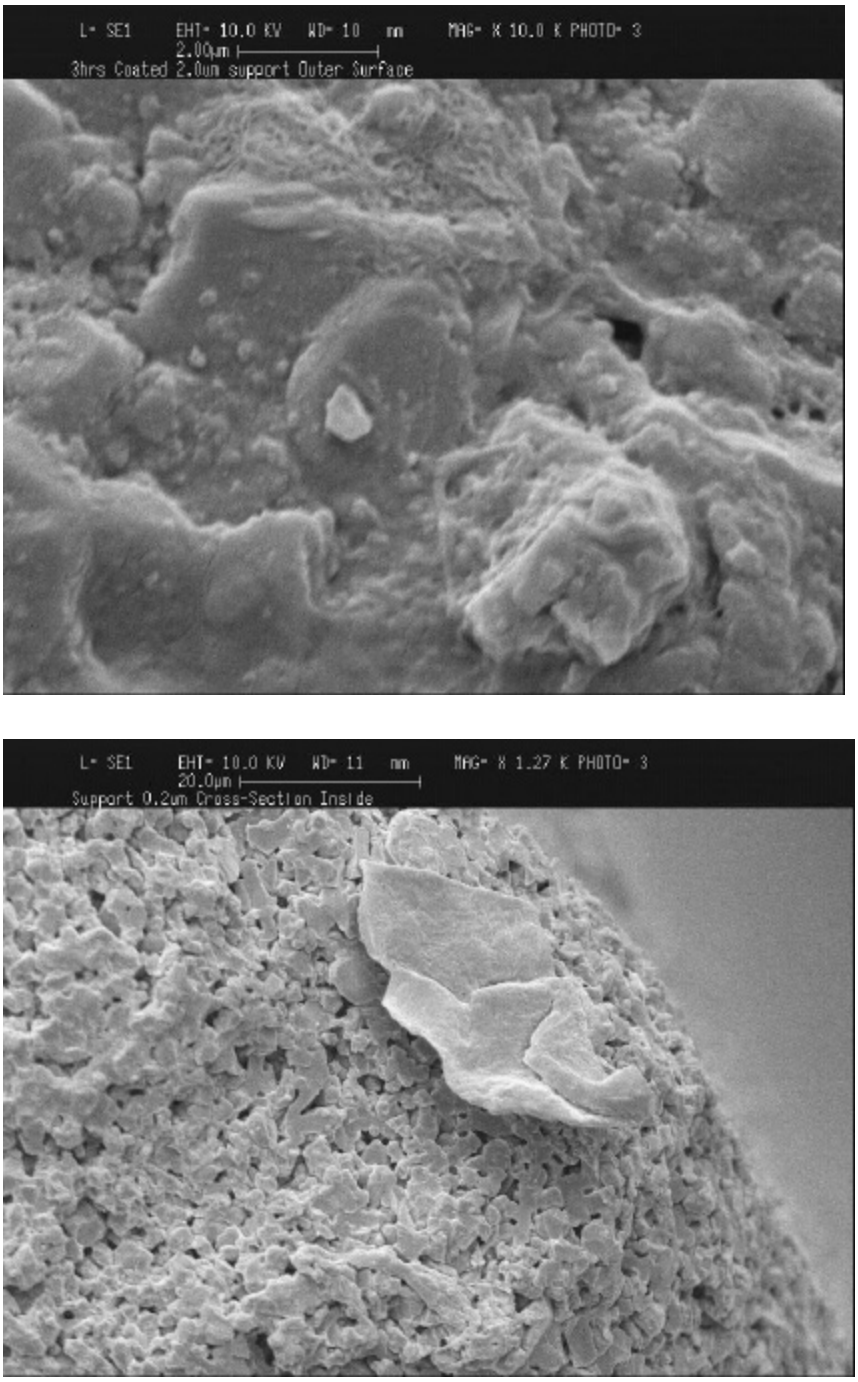

Figure 4.5 SEM Photomicrograph of the outer tubular surface (top) and cross section (bottom) of the 0.2µm substrate. Pore plugging by the hydrotalcite is evident under this higher magnification on the outer surface but not in the cross section.

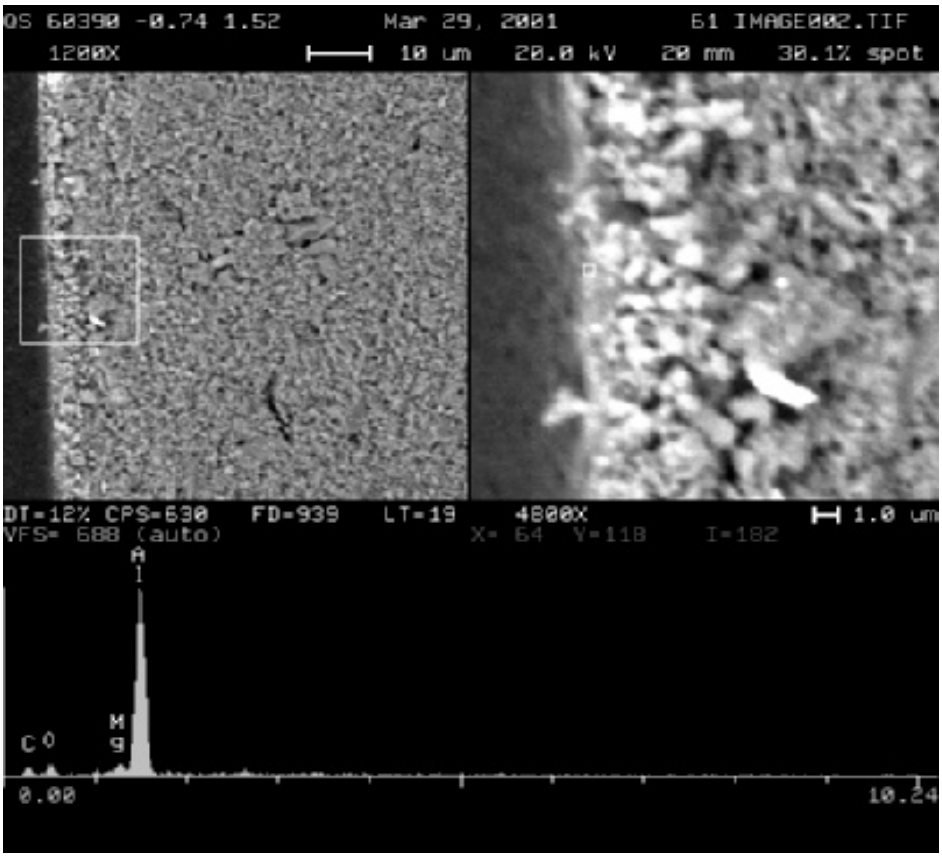

Figure 4.6 SEM photomicrograph and EDX of the outer surface of the 500Å substrate after in-situ crystallization of hydrotalcite. The presence of Mg confirms the formation of hydrotalcite on the outer tubular surface.

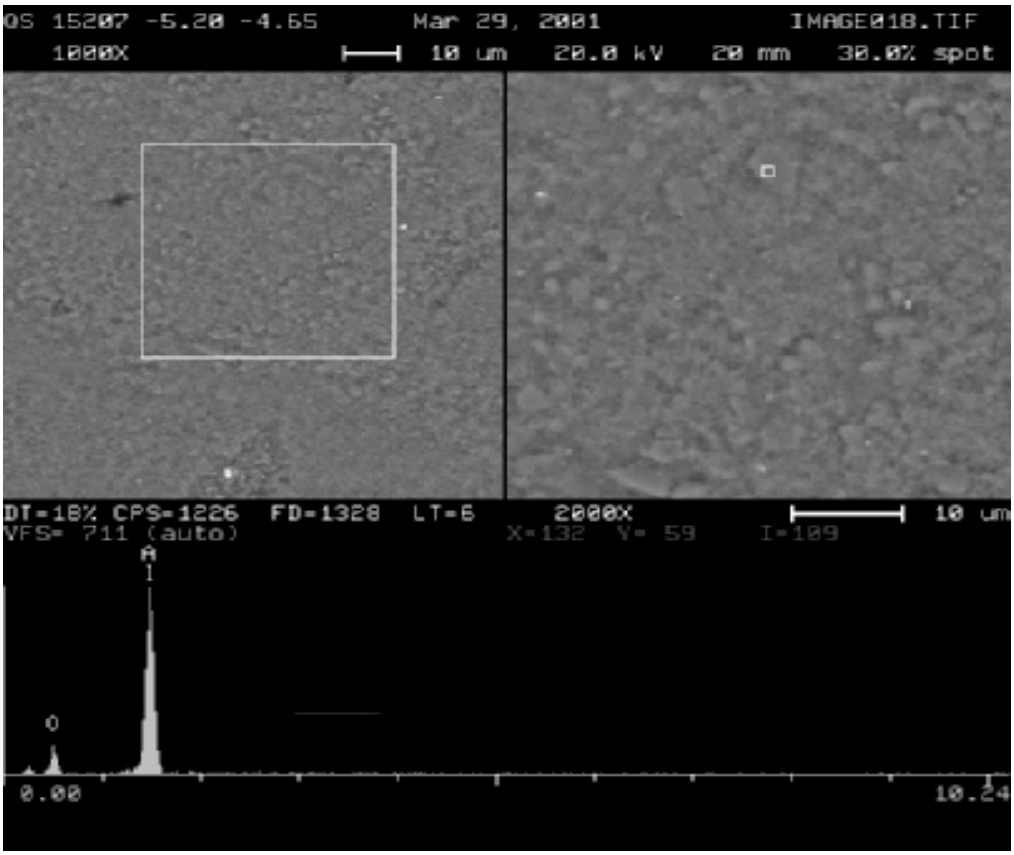

Figure 4.7 SEM Photomicrograph and EDX focused on one of the substrate particle. No Mg was detected. Combining the result from Figure 4.6 verifies that in-situ crystallization takes place within the porous structure of substrate, not on the top of the substrate.

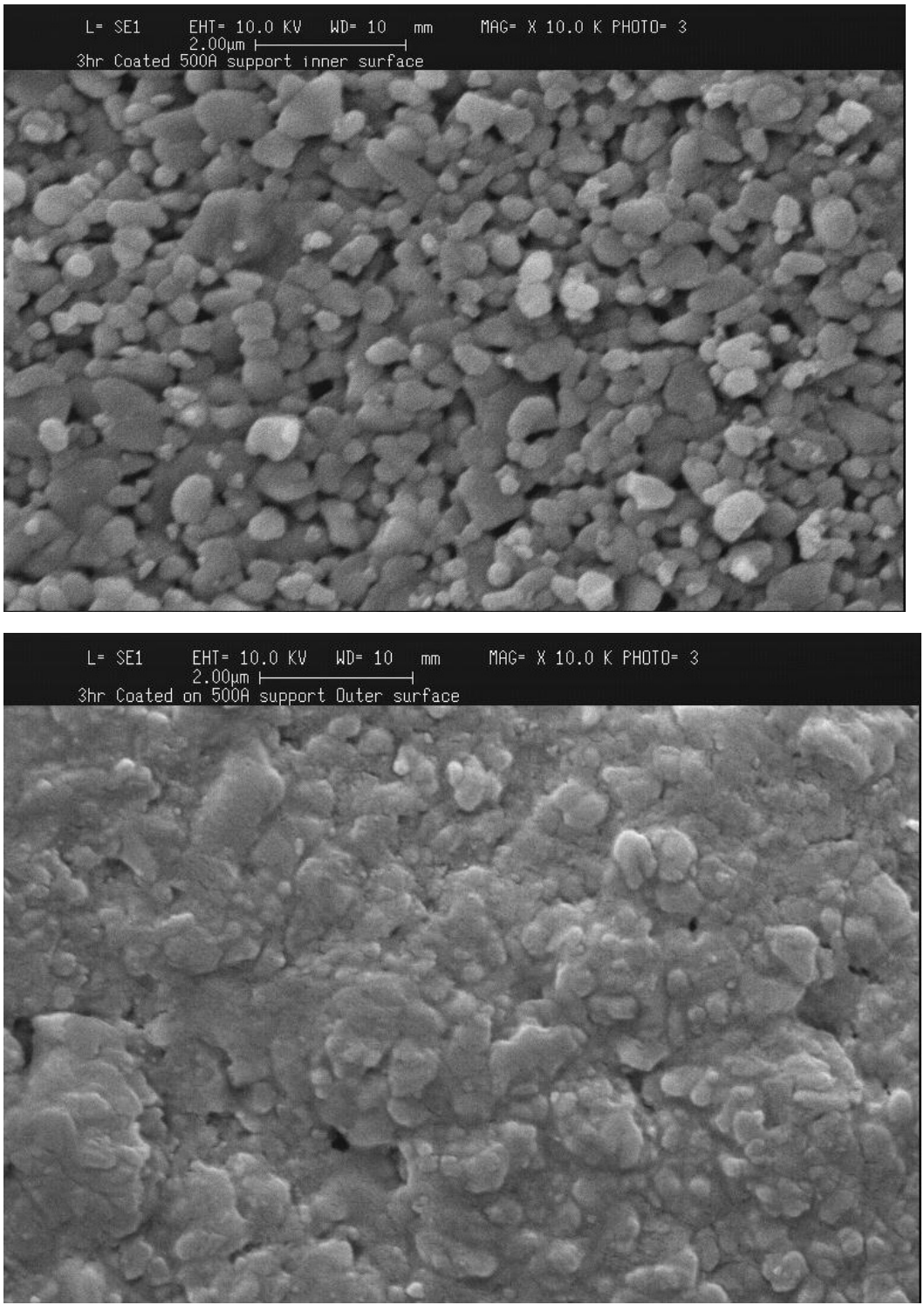

Figure 4.8 SEM Photomicrograph of 500Å substrate after in-situ crystallization of hydrotalcite: Inner tubular surface (top), and outer tubular surface (bottom). Pore plugging by hydrotalcite on the outer tubular surface is evident.

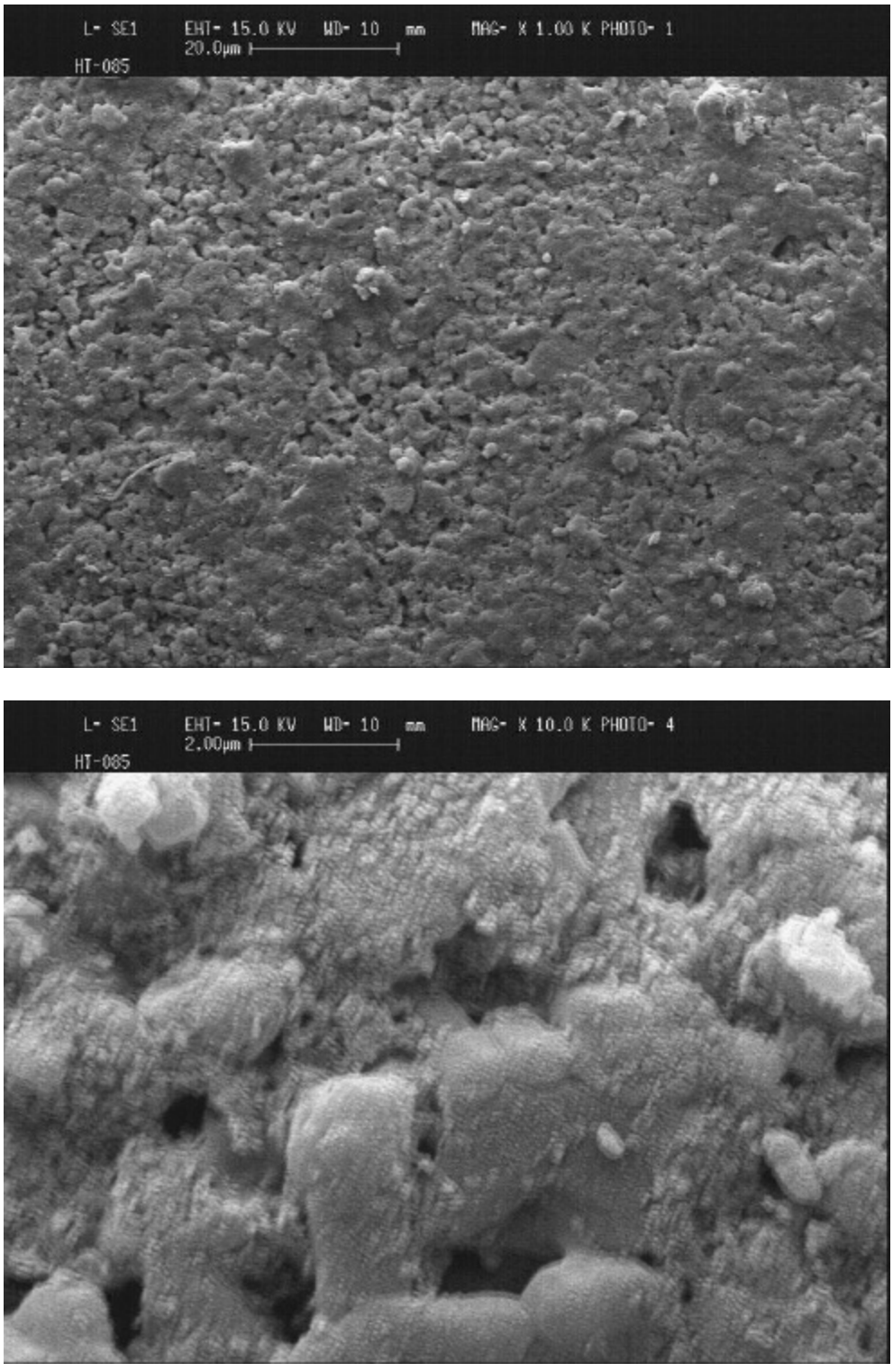

Figure 4.9 SEM photomicrograph for hydrotalcite membrane prepared Via impregnation: 1st deposition (Top: 1K mag, Bottom: 10K mag)

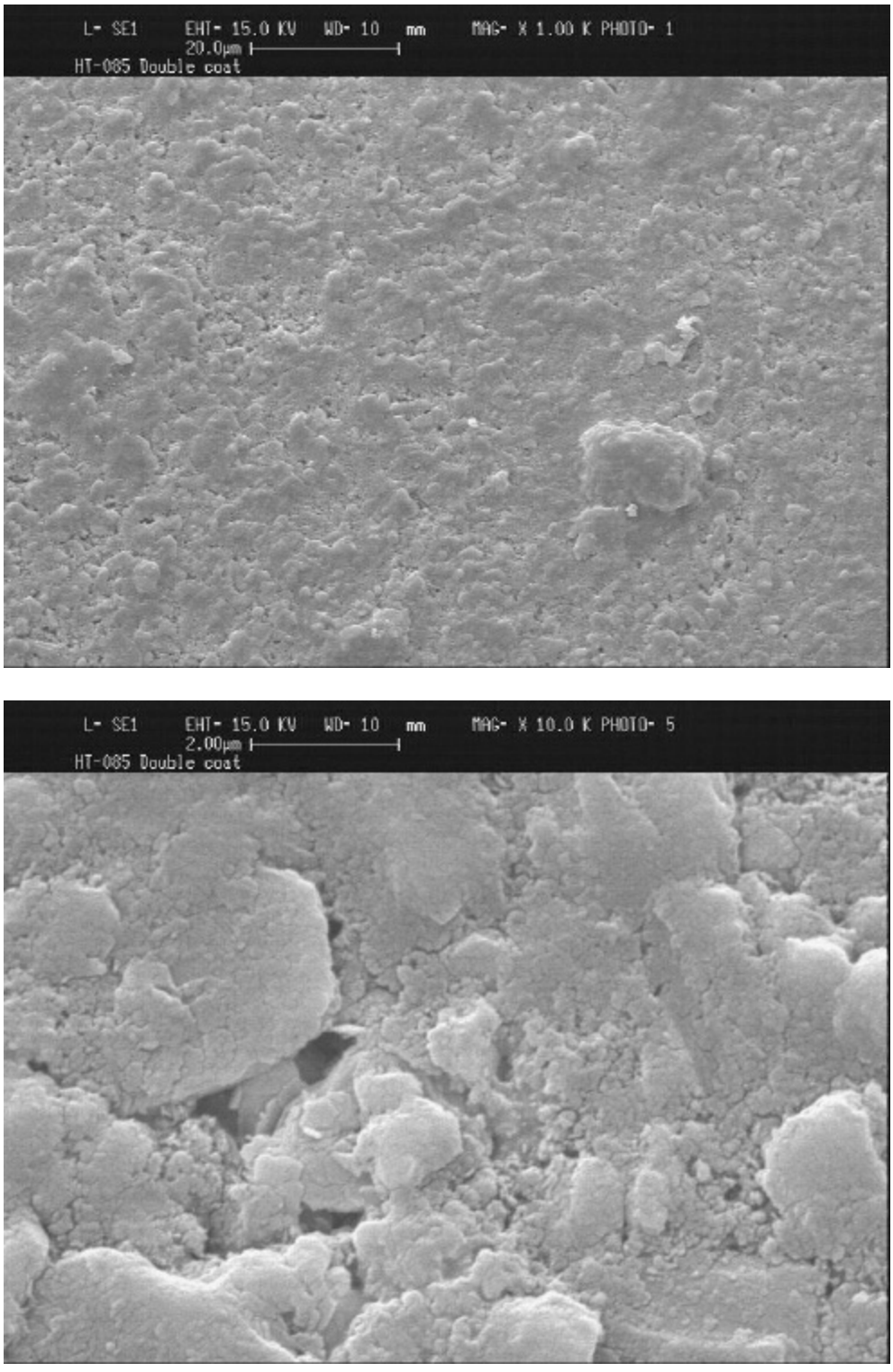

Figure 4.10 SEM photomicrograph of hydrotalcite membrane prepared via impregnation: 2nd deposition (Top: 1K mag, bottom: 10K mag)

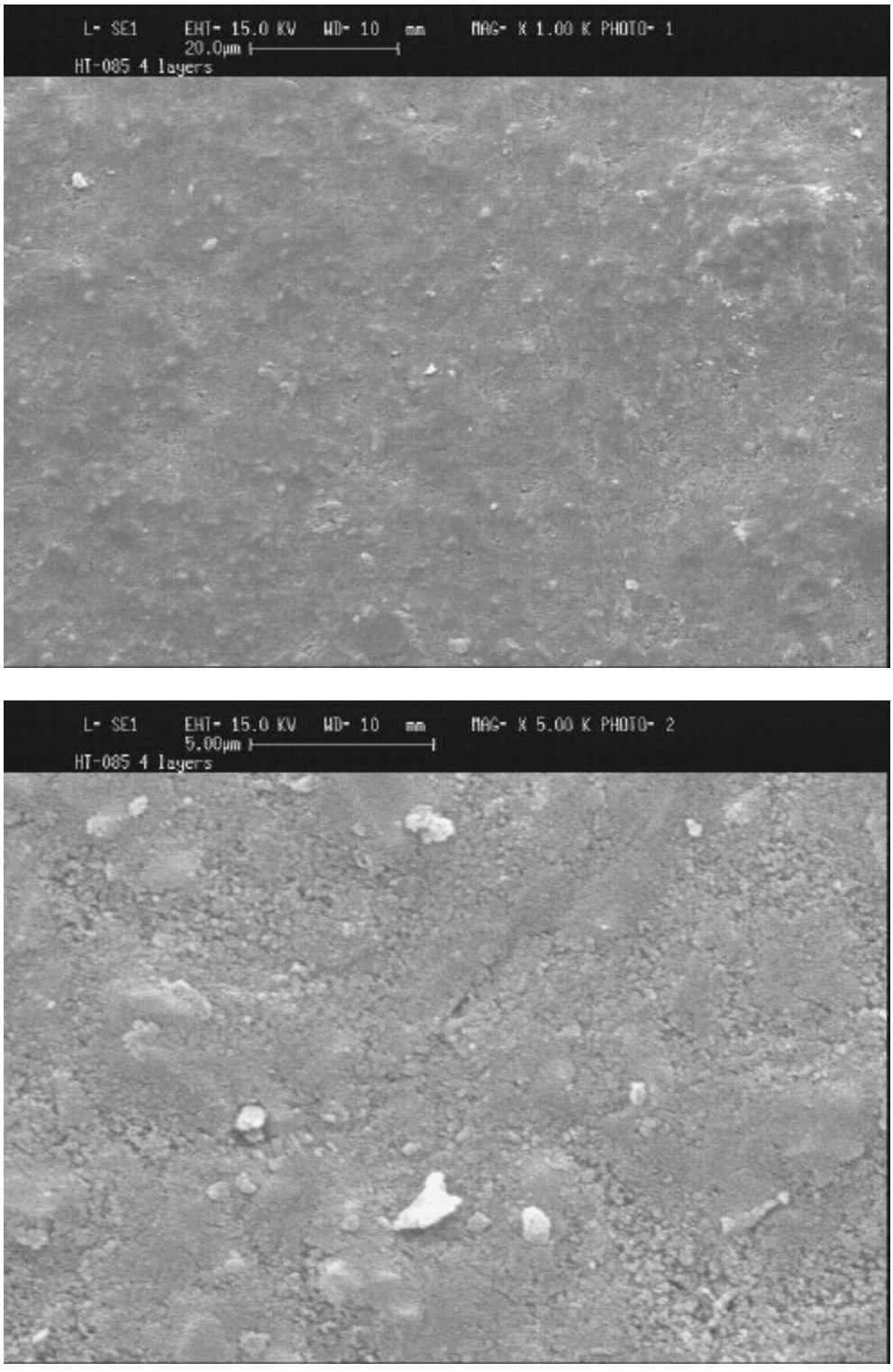

Figure 4.11 SEM photomicrograph of hydrotalcite membranes prepared from impregnation (4 times). Magnification: 1K top, 5K bottom.

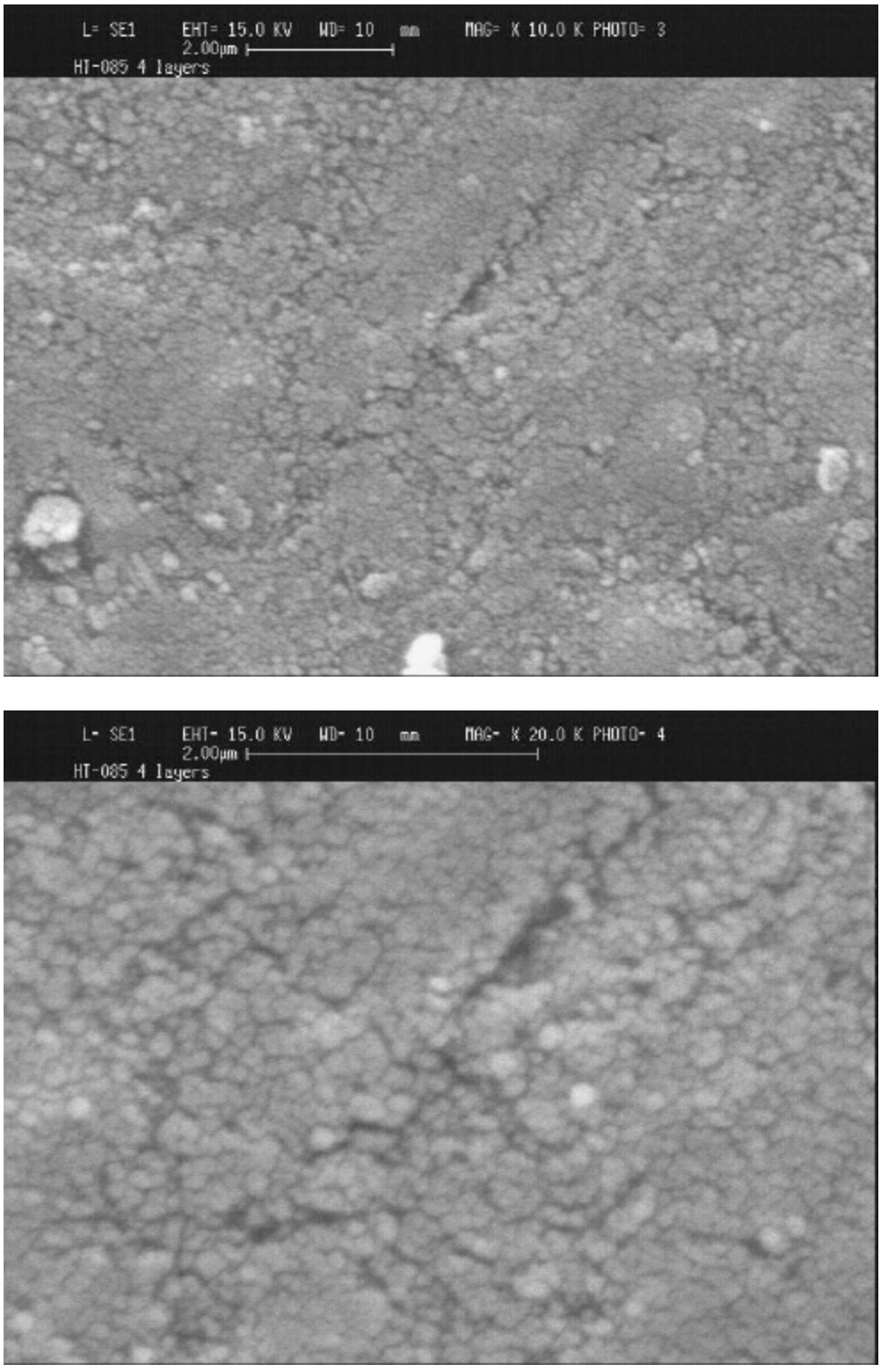

Figure 4.12 SEM photomicrograph of hydrotalcite membranes prepared from in-situ crystalization (4 times) on the 0.2µm Al_2O_3 membrane. Magnification: 10K top, 20K bottom.

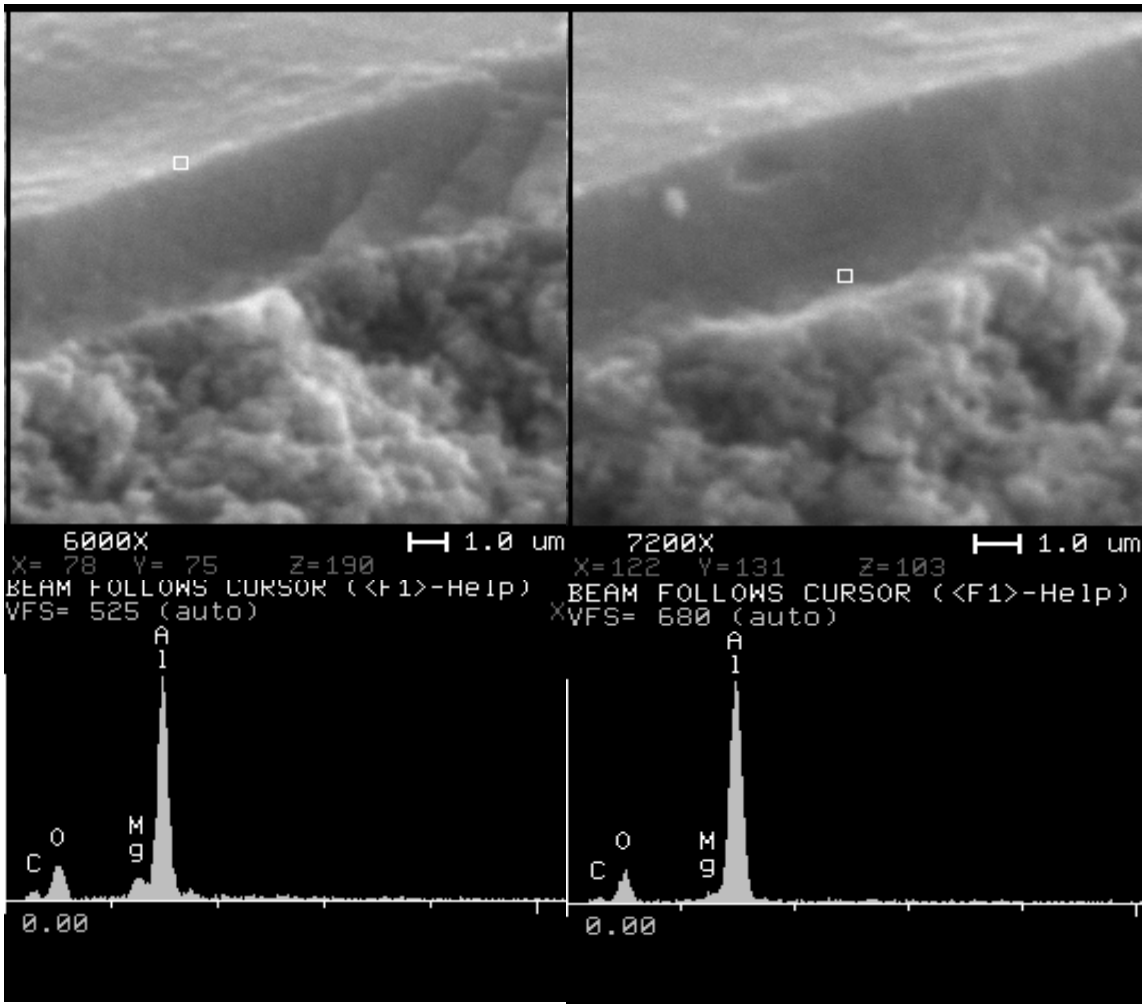

Figure 4.13 SEM and EDX profiles of hydrotalcite membrane deposited on the 40Å substrate.

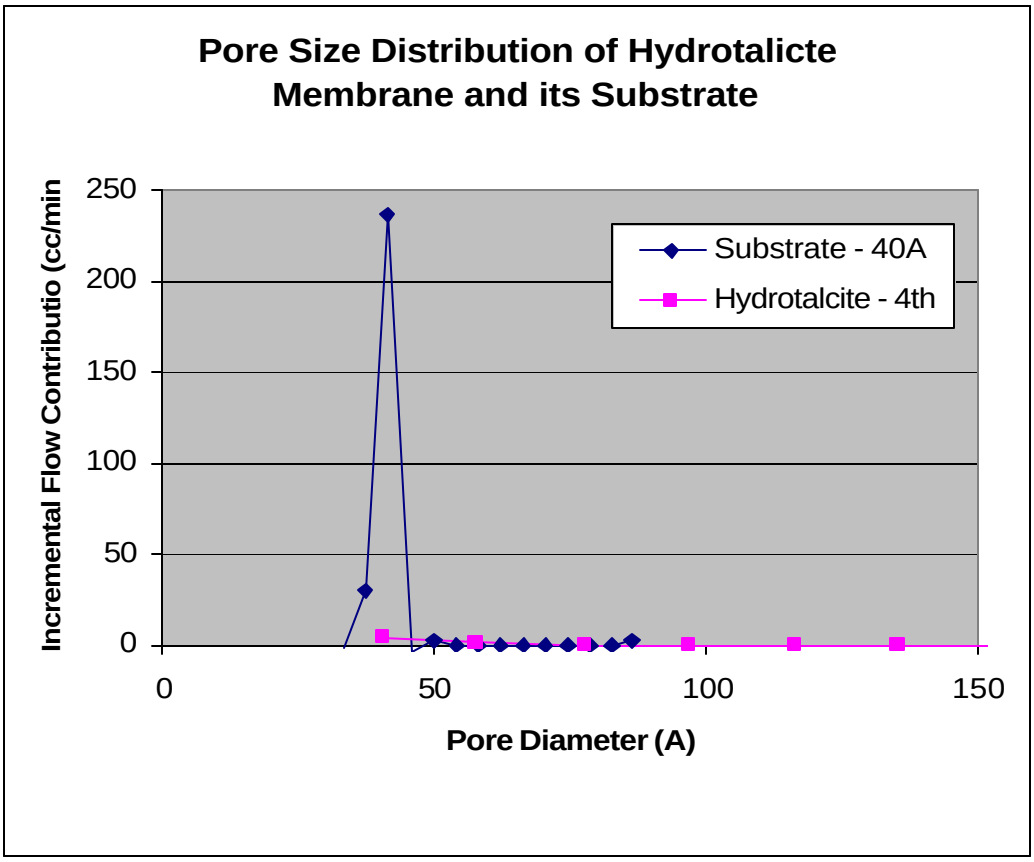

Figure 4.14 Pore size reduction of the ceramic membrane with 40Å pore size after deposition of hydrotalcite via in-situ crystallization.

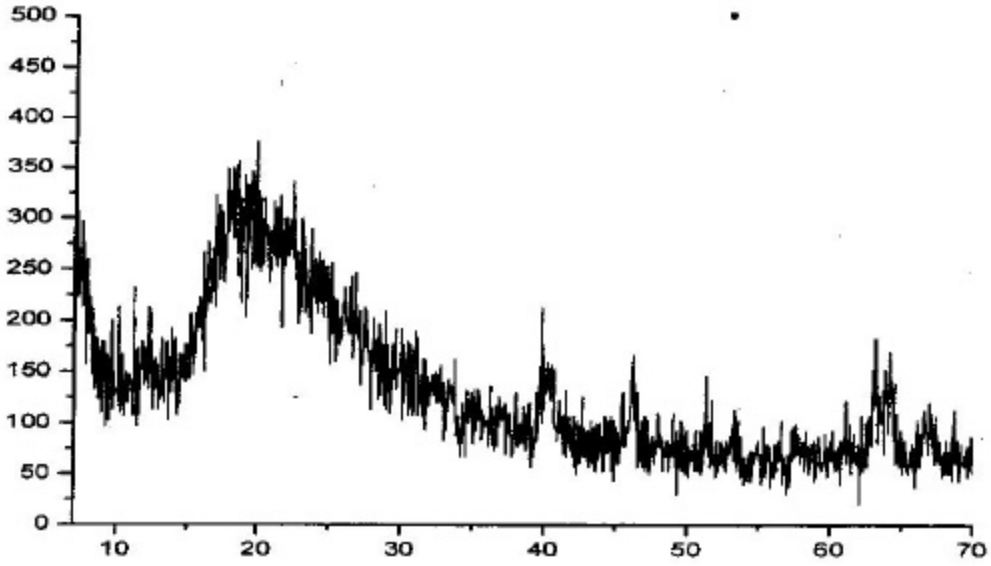

Figure 4.15 XRD of hydrotalcite membrane synthesized via in-situ crystallization.

4.3 Hydrotalcite Membrane Synthesis via Slip Casting

As illustrated in Figure 4.16, slip casting of the hydrotalcite thin film is not different from the slip casting of existing mesoporous $A1_2O_3$ membranes (with pore size in the range of 40Å to <0.2µm). The critical parameters for this approach include the preparation of the slip with (i) a proper particle size, and (ii) appropriate rheology. Thus, a defect free thin film can be deposited on the surface of the membrane without defects after thermal annealing. Our goal here is to deposit a thin film of hydrotalcite with ~100Å pore size; then CVD/I technique can be applied to seal the opening in this range.

4.3.1 Experimental

- *Particle Size of Slip*…Hydrotalcite precipitates were prepared from the precursor chemicals, which was then compared with the particle size of our commercial mesoporous membranes (0.2µm or less in pore size). The hydrotalcite particles comparable with the particles size of the Al_2O_3 membranes was selected for the preparation of the slip.

- *Rheology of Slip*…The formula for the preparation of the mesoporous Al_2O_3 membrane was modified for our purpose here.

4.3.2 Results and Discussions

- *Particle Size of Hydrotalcite Slip*…According to our experience with Al_2O_3, the particle size required to form this range of pore size is in the neighborhood of 500 to 800Å as shown in Figure 4.17. Particles from the hydrotalcite gel are in fact smaller than this range and appear very uniform in size as shown in Figure 4.17. Based upon this observation, we believe that the hydrotalcite gel we prepared satisfies the first requirement in terms of the particle size.

- *Rheology of Hydrotalcite Slip*…As far as the rheology of the slip is concerned, we found that, without the modification of the viscosity of the sol, the layer quality was very poor. Our first attempt is to adapt the gel formula we use to prepare the Al_2O_3 thin film for our purpose. The result from this attempt appears very promising. The membranes with the 1, 2, and 3- layer casting have been prepared and well characterized. Each membrane was calcined at 400ºC before the characterization. Figures 4.18 & 4.19 show the membrane with one layer casting. The hydrotalcite evidently covered most opening of the substrate. However, some uncovered defects were observed. Figures 4.20 & 4.21 show the membranes with the two-layer casting. The quality was improved significantly. It is clear that the particles formed by the gel are very uniformly and evenly deposited on the surface of the substrate. Figures 4.22 & 4.23 show the membrane with the 3-layer deposition. It appears that the layer quality is not improved; in fact, it shows some missing spots possibly due to its thickness. The

permeance was measured for the 1, 2 and 3 layer membrane, which are presented in Table 4.3. About 50% permeance reduction was achieved with the 1-layer casting. The permeance after the 1st layer was not reduced noticeably, consistent with the observation from the SEM. Figure 4.24 shows the membrane prepared with two layers. However, this sample was calcined between the layers. Some micro crack was observed and its layer quality was not improved. Thus, we conclude from this study that the two-layer casting appears sufficient to prepare a uniform membrane. As shown in Table 4.3, the hydrotalcite membrane prepared with the 2-layer casting appears comparable to the existing 100Å membrane based upon the permeance.

- *Characterization of the Green Layer*…As indicated above, the green layer formed with the improved formula appeared defect free according to SEM examination. We also conducted initial flow analysis using helium flow saturated with water at room temperature. According to our previous experience, no initial flow can be detected for an Al_2O_3 membrane with 100Å commercially available from us. The initial flow measurements from the two samples are presented in Table 4.4. It is believed that the green layer after drying at 80°C is nearly defect free as indicated by the very low initial flow for both 94-7-1/2 and 94-7-1. Drying at 200°C increases the initial flow slightly, i.e., from 1.6 to 6.4%; however, this increased level of initial flow is considered within the tolerance of the micro porous membrane. Calcination at 300°C apparently significantly increased the initial flow, i.e.. ~87%, indicative of the layer collapse. Hydrotalcite began to release its interlayer water approaching 200°C according to TGA. Thus, the layer shrank during the calcinations; however, when the layer exposed to the initial flow testing, the layer re-expanded, causing major defects throughout the layer.

Table 4.3 Characterization of Green Layer of Hydrotalcite Deposited via Slip Casting

Sample ID	Calcination Temperature ©	Initial Flow (%)	Selectivity (He/N_2)
94-7-1/2-1	80	3.6	1.98
94-7-1/2-2	80	1.6	1.76
	200	6.4	1.83
94-7-1-1	80	1.5	1.89
	200	0.97	1.82
	300	87[1]	1.91
94-7-1-2	80	2.0	1.78

Table 4.4 Permeance of Membranes prepared via Slip Casting

Sample ID	He Permeance [$m^3/m^2/hr/bar$]	N2 Permeance [$m^3/m^2/hr/bar$]	Selectivity
HT 94-02 -1 layer	69.85	33.54	2.08
HT 94-02 -2 layer	65.54	33.74	1.90
HT 94-02 -3 layer	64.81	35.41	1.83
Control M & P 100Å	87	40	2.18

- Composition of slip, particularly binder/HT ratio.
- Particle size to form porous thin film suitable for CVD backpatching

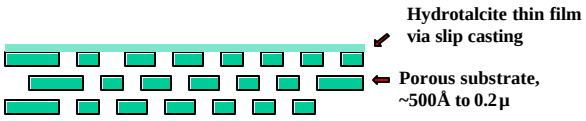

Figure 4.16 Concept on hydrotalcite membrane synthesis via slip casting.

[1] The initial flow went through a minimum, i.e., <1%, and then increased to this level throughout the measurement.

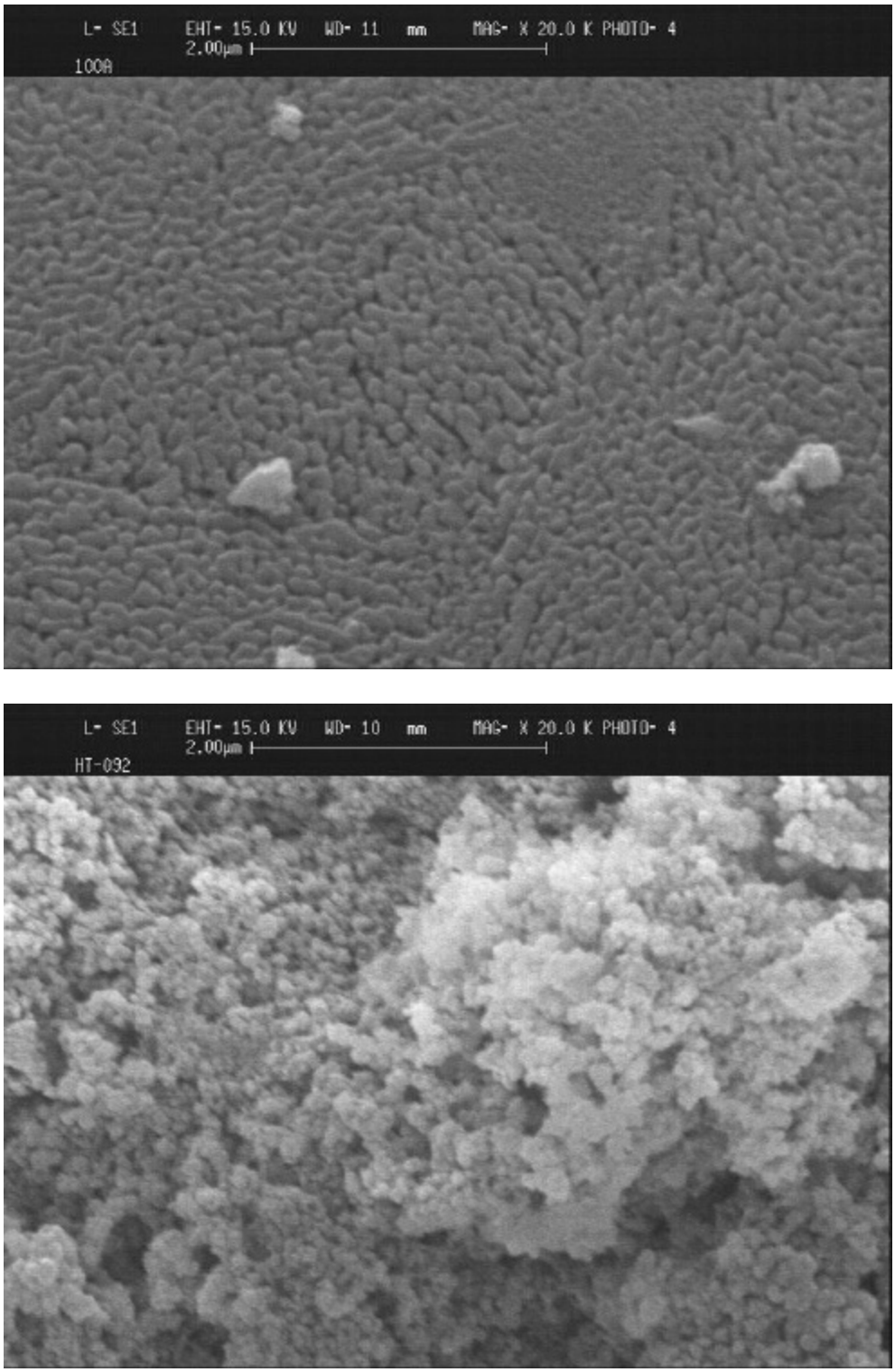

Figure 4.17 Particle size comparison between M&P's commercial ceramic membrane with 100Å pore size (top) vs hydrotalcite gel prepared by us (bottom).

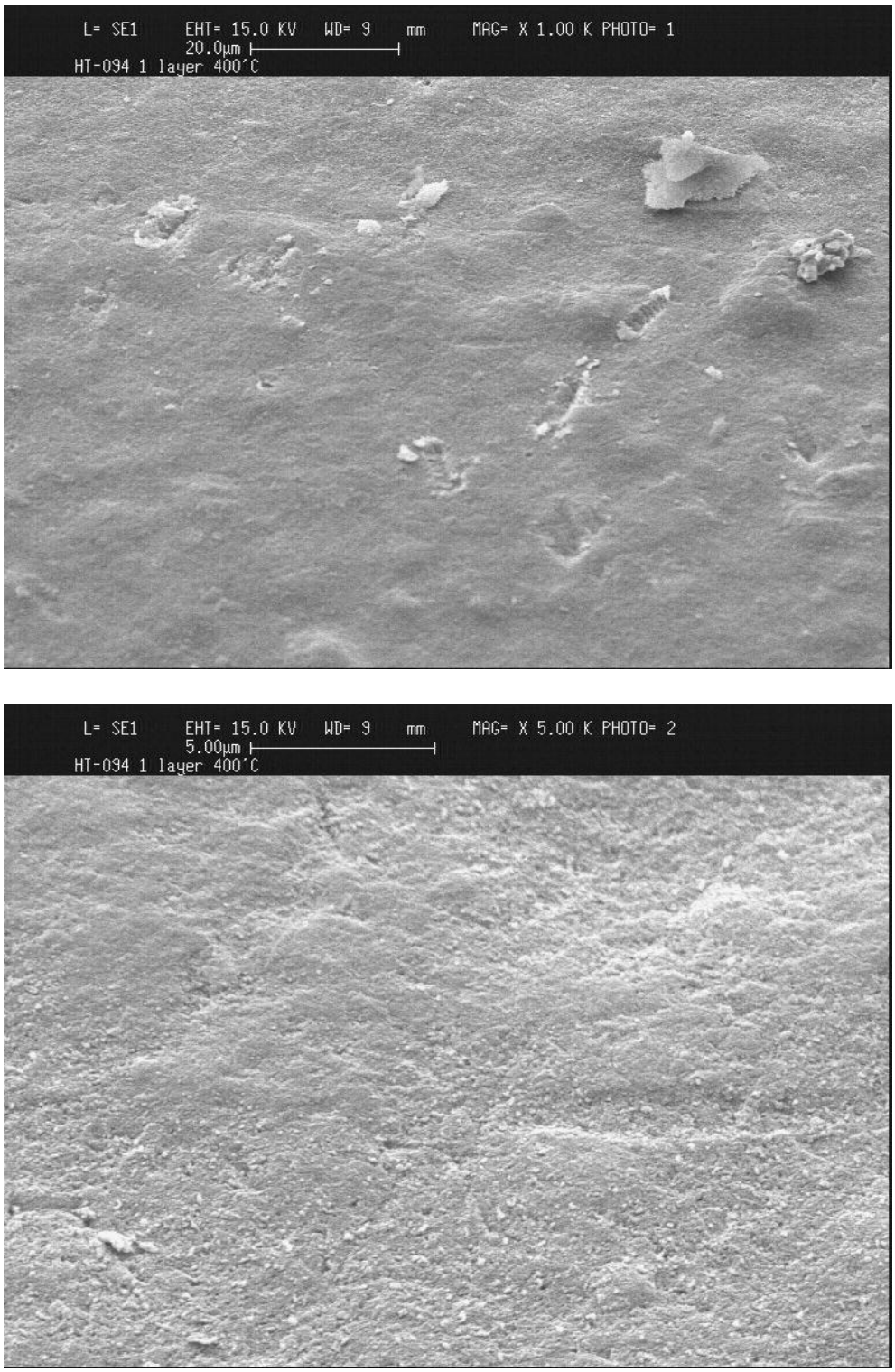

Figure 4.18 SEM photomicrograph of hydrotalcite membrane prepared from Slip casting: one layer casting and then calcined at 400ºC (Top: 1 K mag, Bottom: 5K)

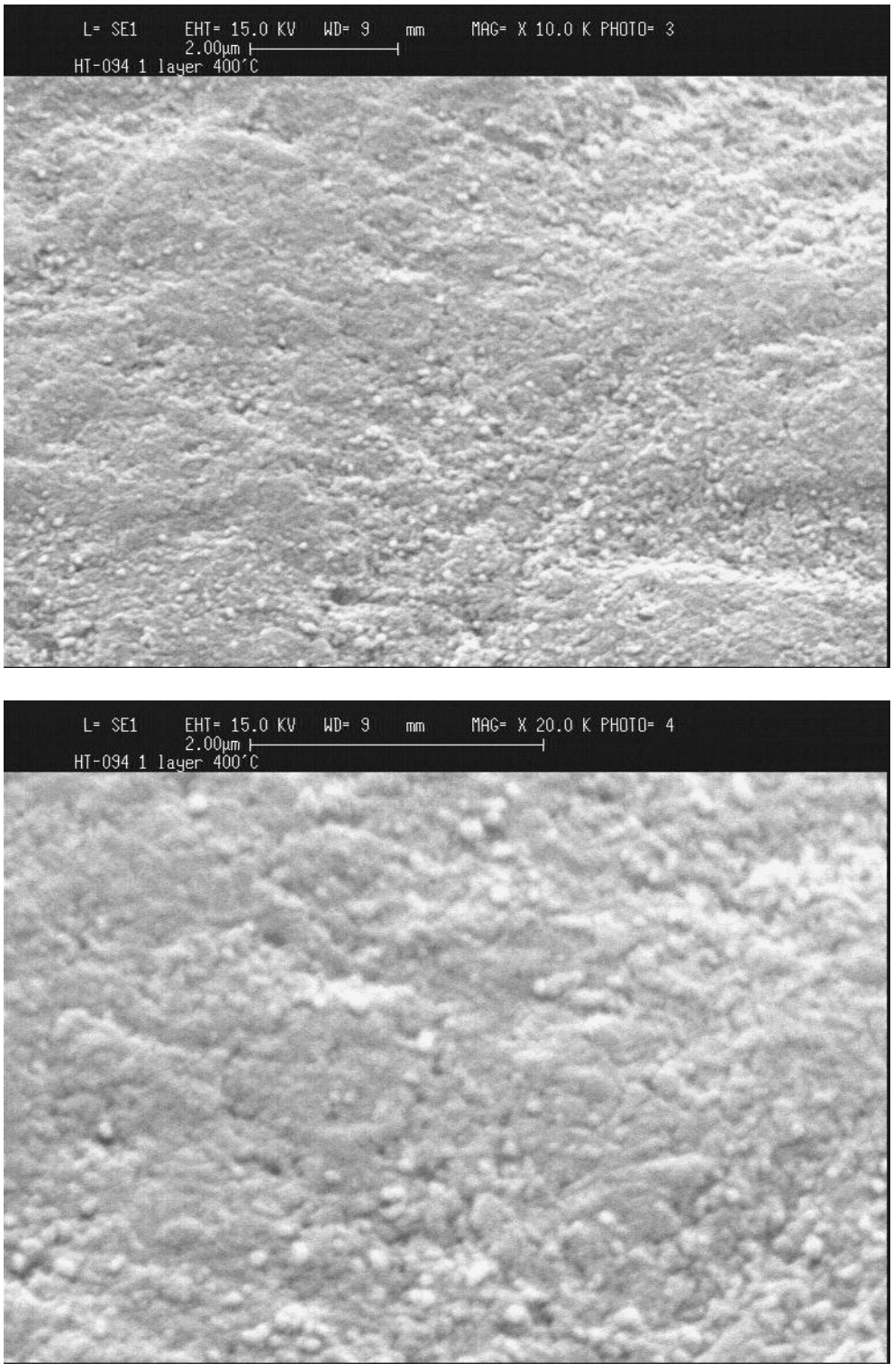

Figure 4.19 SEM photomicrograph of hydrotalcite membrane prepared from slip casting: one layer casting and then calcined at 400ºC (Top: 10 K mag, Bottom: 20K)

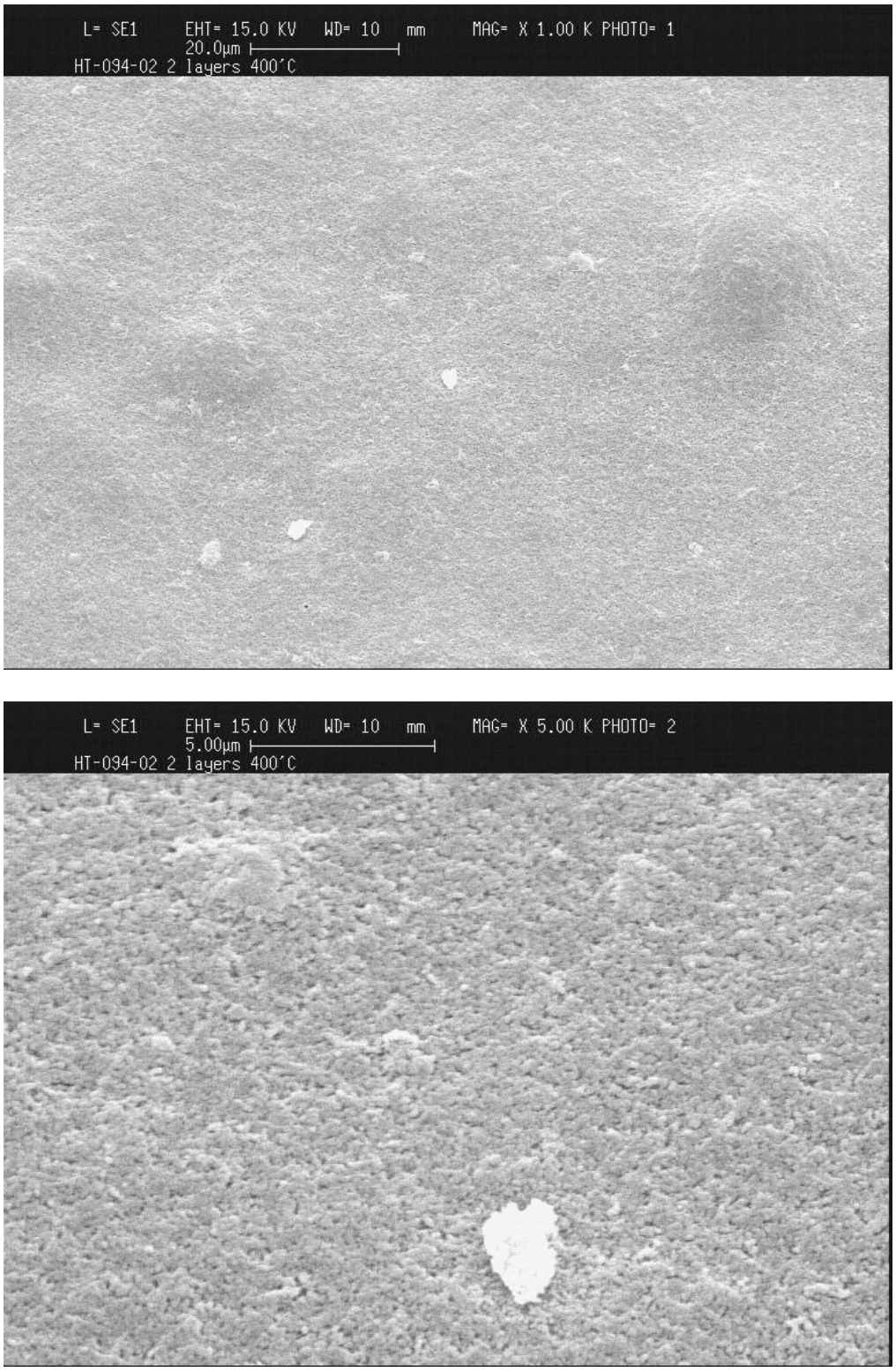

Figure 4.20 SEM photomicrograph of hydrotalcite membrane prepared from slip casting: two-layer casting and then calcined at 400ºC (Top: 1 K mag, Bottom: 5K mag)